https://doi.org/10.5194/egusphere-2025-3620
Preprint. Discussion started: 6 October 2025

Prognostic simulations of mixed-phase clouds with model 1D-AC v1.0: The impact of freezing parameterizations on ice crystal budgets

Yijia Sun[1], Ann M. Fridlind[2], Israel Silber[3], Nicole Riemer[4], Daniel A. Knopf[1]
[1]Stony Brook University, Stony Brook, NY 11794, USA
[2]NASA Goddard Institute for Space Studies, New York, NY 10025, USA
[3]Pacific Northwest National Laboratory, Richland, WA 99352, USA
[4]University of Illinois at Urbana-Champaign, Urbana, IL 61801, USA

Correspondence to: Daniel A. Knopf (daniel.knopf@stonybrook.edu)

Abstract. Mixed-phase clouds at high latitudes contribute to the uncertainty in predicting cloud feedbacks and climate sensitivity, mainly due to the complexity of microphysical processes that influence the partitioning between the supercooled liquid and ice phases, and hence, cloud radiative effects on regional scales. Particularly in Arctic mixed-phase clouds, the activation of ice-nucleating particles (INPs) from various aerosol populations remains a leading source of uncertainty. Our study employs a one-dimensional aerosol-cloud model informed by large-eddy simulations to probe the impact of INP representation on predicted ice crystal number concentrations (N_i) and ice crystal budgets in mixed-phase Arctic stratus. We apply three immersion freezing (IMF) parameterizations, two time-independent (deterministic) and one time-dependent (classical nucleation theory), to predict the evolution of the INP reservoir and resulting ice crystal budget from polydisperse mineral dust, organic (humic-like substances), and sea spray aerosol particle size distributions. Our analysis focuses on how variations in aerosol number concentration and cloud system parameters such as cloud cooling rate, cloud-top entrainment rate, and ice crystal fall speed influence the INP reservoir and ice crystal budgets. Furthermore, this study investigates the competitive ice nucleation dynamics in mixed aerosol environments and provides a process-level quantification of the INP budget terms, which directly controls ice crystal budgets. For all studied case scenarios, the aerosol types and associated particle size distributions significantly impact INP and N_i, and the choice between a time-dependent and a deterministic freezing description yields orders-of-magnitude differences in the predicted INP and N_i over the 10 h simulation time, reflecting typical cloud lifetimes. Our results show that the influence of cloud cooling, INP entrainment, and sedimentation varies significantly depending on the chosen freezing parameterization. These findings underscore the critical need for robust IMF parameterizations and precise cloud system observations to enhance the accuracy of models in predicting mixed-phase cloud structure and evolution.

https://doi.org/10.5194/egusphere-2025-3620
Preprint. Discussion started: 6 October 2025

1 Introduction

In the Arctic regions, the rate of warming has been at least twice as large as the global mean since pre-industrial times (Holland et al., 2003; Serreze et al., 2011; Gulev et al., 2021), a phenomenon known as "Arctic amplification" (Hahn et al., 2021; Morice et al., 2021) that coincides with a drastic decrease in the cover of sea ice (Stroeve et al., 2012; Richter-Menge, 2018). Stratus, a predominant cloud type in polar regions (Shupe et al., 2008; Shupe, 2011; Andronache, 2018; Lubin et al., 2020), plays a crucial role in the surface and top-of-atmosphere radiative budget due to its extensive prevalence (eg., Dong et al., 2003; Zuidema et al., 2005). These clouds control the development of precipitation through their liquid and ice phases (eg., Field et al., 2015; Mülmenstädt et al., 2015; Korolev et al., 2017; Silber et al., 2021). Arctic stratus clouds are predominantly mixed-phase clouds (MPCs) (Curry et al., 2000; Korolev et al., 2003; Shupe, 2011), characterized by the presence of at least one supercooled liquid water layer where ice crystals form and sediment subsequently (Shupe et al., 2006; Morrison, 2012; Silber et al., 2021). The persistence of this mixed-phase state is governed by a delicate interplay between cloud dynamics and microphysics, with the ambient ice concentration determining whether the cloud remains liquid-bearing or glaciates (Khain et al., 2022).

In these Arctic MPCs, ice formation typically occurs from the supercooled liquid phase through heterogeneous ice nucleation. Heterogeneous ice nucleation can commence via several modes including immersion freezing (IMF), where freezing is initiated on the surface of an ice-nucleating particle (INP) that is immersed in a supercooled aqueous solution droplet (Vali et al., 2015). Recent studies have indicated that IMF is the dominant pathway of primary ice formation in MPCs (Ansmann et al., 2008; Prenni et al., 2009; Hoose et al., 2010; De Boer et al., 2011; Hoose et al., 2012b; Murray et al., 2012; Westbrook et al., 2013; Kanji et al., 2017; Silber et al., 2021; Burrows et al., 2022).

To accurately predict the number concentration of ice nucleating particles (INPs) from aerosol particles, IMF parameterizations are needed. Over the past decades, IMF parameterizations representing specific particle types have been developed (Bauer et al., 2008; Murray et al., 2012; Niemand et al., 2012; Knopf et al., 2013; Demott et al., 2015; Liu et al., 2016; China et al., 2017; Kanji et al., 2017; Knopf et al., 2018; Mccluskey et al., 2018; Penner et al., 2018; Alpert et al., 2022; Burrows et al., 2022; Knopf et al., 2023a). Typically applied freezing parameterizations include deterministic schemes based on the singular hypothesis (Levine, 1950; Vali, 1971; Vali, 2014), and stochastic schemes, such as those based on classic nucleation theory (CNT) (Pruppacher et al., 2010; Knopf and Alpert, 2023a).

Deterministic IMF parameterizations are founded on the assumption that ice nucleation active sites (INAS) initiate ice nucleation instantaneously when a specific temperature is reached for each INAS on an immersed particle surface. This freezing efficiency can therefore be described as a function of temperature and particle type including particle number concentration and size. The deterministic description is thus time independent, thereby neglecting the cooling rate dependence in ice nucleation observations (Bigg, 1953; Pruppacher and Klett, 2010; Alpert et al., 2016; Knopf et al., 2020; Arabas et al., 2025).

https://doi.org/10.5194/egusphere-2025-3620
Preprint. Discussion started: 6 October 2025

The CNT-based parameterizations make no claim of specific INAS initiating freezing but assume that ice nucleation proceeds stochastically on the INP surface, and increasing INP surface area will therefore increase the freezing rate (Pruppacher and Klett, 2010; Knopf et al., 2020; Knopf and Alpert, 2023a). As such, CNT-based parameterizations are time dependent. As a consequence, at constant supersaturation with respect to ice, as time progresses, more freezing events are observed in accordance with experimental studies (e.g., Biermann et al., 1996; Koop et al., 1997; Alpert and Knopf, 2016; Knopf et al., 2020; Deck et al., 2022).

Mineral dust, organic, and sea spray aerosol (SSA) particles are common aerosol types in the Arctic region (Udisti et al., 2020; Schmale et al., 2021). At temperatures below -20 °C, mineral dust has a particularly high ice nucleating efficiency (Kanji et al., 2017) and is assumed to be the best understood source of INPs (Burrows et al., 2022). The variability of atmospheric INP concentrations can, in cases, be attributed to the change in number concentration of long-range transported dust (Demott et al., 2003; Chou et al., 2011; Boose et al., 2016; Burrows et al., 2022; Shi et al., 2022; Kawai et al., 2023). Organic aerosol (OA) particles can be directly emitted from fossil fuel combustion and biomass burning, also termed primary organic aerosol (POA). The condensation of oxidized volatile organic compounds (VOCs) can yield secondary organic aerosol (SOA) particles (Hallquist et al., 2009; Shrivastava et al., 2017; Bergman et al., 2022; Srivastava et al., 2022). The organic matter (OM) associated with OA particles that initiate the ice nucleation in the atmosphere is still not well understood (Knopf et al., 2018). OM can exhibit various phase states at the same atmospheric thermodynamic conditions, resulting in different ice nucleation pathways and ice nucleation rates (Knopf et al., 2018). Through recent field measurements and laboratory investigation, it has been pointed out that particulate OM can contribute to atmospheric ice nucleation (Knopf et al., 2010; Wang et al., 2012a; Wang et al., 2012b; Hiranuma et al., 2013; Knopf et al., 2014; Alpert and Knopf, 2016; Knopf et al., 2020; Xue et al., 2024). Several studies have demonstrated that in remote marine regions far from the influence of continental INP sources, SSA particles can act as a significant INP source (Burrows et al., 2013; Wilson et al., 2015; Vergara-Temprado et al., 2017; Huang et al., 2018; Mccluskey et al., 2018; Mccluskey et al., 2019; Zhao et al., 2021; Alpert et al., 2022; Raatikainen et al., 2022; Xue et al., 2024). Soot particles, which have also been discussed as a potential source of anthropogenic INPs. Under polluted conditions, relatively high black carbon fraction has been found in both cloud residuals as well as simulated results (Savre et al., 2015). However, recent laboratory studies reveal that soot exhibits minimal efficacy in immersion-mode freezing (Friedman et al., 2011; Schill et al., 2018; Kanji et al., 2020; Schill et al., 2020). Its contribution to atmospheric ice formation at temperatures above −38°C is likely not significant (Kanji et al., 2020).

In addition to ambient particle types, typical aerosol particle size distributions (PSDs) present in the Arctic are relevant to ice formation rates. The PSDs determine the particle number and surface area concentration, a necessary input for the IMF parameterizations, thus influencing the number concentration of INPs and, ultimately, ice crystals. In this study, we apply the PSDs derived from Indirect and Semi-Direct Aerosol Campaign (ISDAC) (Earle et al., 2011; Hiranuma et al., 2013) and the International Chemistry Experiment in the Arctic LOwer Troposphere (ICEALOT) (Quinn et al., 2017), both carried out in the Arctic region. Detailed information can be found in the methods section.

https://doi.org/10.5194/egusphere-2025-3620
Preprint. Discussion started: 6 October 2025

Our study is motivated by the fact that the inferred strength of ice production within Arctic stratus MPCs has often been challenging to reproduce by models applying a prognostic INP treatment, i.e., a treatment where the budget of INP is tracked (Harrington et al., 2001; Morrison et al., 2005; Fridlind et al., 2007; Fan et al., 2009; Avramov et al., 2011; Fridlind et al., 2012). Such a treatment contrasts with simpler diagnostic treatments of INP that enable physically unrealistically high ice formation rates to persist indefinitely (e.g., Knopf et al., 2023b), and our previous work indicates that the type of IMF parameterization (deterministic or CNT-based) plays an important role in the strength of ice formation rates under Arctic stratus conditions (Knopf et al., 2023b; Arabas et al., 2025). In general, when assuming a deterministic freezing scheme, INP depletion from a turbulently mixed stratus layer occurs within a short period of time, on the order of the mixing time for a well-mixed cloud-topped boundary layer. This rapid depletion results from the INP exposure (via turbulent transport) to conditions that result in their instantaneous activation at the coldest conditions within the cloud layer (within cloud tops). Subsequently, cloud-top entrainment or cooling as drivers of INP activation have often appeared too weak to explain observed ice crystal loading (Fridlind et al., 2012; Westbrook and Illingworth, 2013). Other processes may contribute to sustaining INP under some specific conditions, such as entrainment of INP from below the turbulently mixed layer if the cloud-containing layer is decoupled from the surface (Avramov et al., 2011) or restoration of some of the activated INP via complete ice crystal sublimation within a turbulently mixed layer if there is an ice-subsaturated layer (at the base) that is deep enough to enable that (Solomon et al., 2015). Under the simplest conditions without such processes possible, Fridlind et al. (2012) demonstrated how unrealistically high concentrations of INPs from the free troposphere were needed to sustain inferred ice production via cloud-top entrainment when applying a deterministic IMF parameterization. Unfortunately, direct constraints on INP budgets have not been possible from available data sets owing at least in part to a lack of INP data within cloud layers, and inferring INP budgets from ice crystal number concentrations invokes an additional set of large uncertainties emerging from all of the factors that influence ice crystal PSDs in Arctic MPCs that must also be parameterized (Fridlind et al., 2007; Avramov et al., 2011; Fridlind et al., 2012; Ovchinnikov et al., 2014; Morrison et al., 2020).

In most previous modelling studies, prognostic ice nucleation has been parameterized with deterministic IMF schemes (Morrison et al., 2005; Avramov et al., 2011; Fridlind et al., 2012; Solomon et al., 2015; Tully et al., 2023). It has been pointed out that such deterministic parameterizations may not be applicable to all atmospherically relevant conditions (temperature and humidity) (eg., Niemand et al., 2012; Hiranuma et al., 2014; Ullrich et al., 2017), partly due to instrument limitations and the limited amount of data collected (Burrows et al., 2022), and this may include slowly continuing ice formation processes that may sustain continuous ice crystal production (Westbrook and Illingworth, 2013; Yang et al., 2013). Several studies have implemented CNT-based parameterizations (Savre and Ekman, 2015; Raatikainen et al., 2022; Shi et al., 2022) to investigate the effects of different INPs on Arctic MPCs. Savre and Ekman (2015) found that the application of an evolving α-PDF scheme (introducing a contact-angle distribution function that scale the freezing efficacy of the INPs) can support continuous in-cloud ice production controlled mostly by the competition between cloud cooling, cloud-top entrainment, and ice sedimentation in three simulated cases. Raatikainen et al. (2022) showed that the relative significance of marine INP emissions and accounting for INP recycling was crucial for maintaining MPCs in their simulations over water rather than ice surfaces. Knopf et al.

https://doi.org/10.5194/egusphere-2025-3620
Preprint. Discussion started: 6 October 2025

(2023b) pointed out another possible explanation that the selection of IMF parameterizations determines the size of the INP reservoir in Arctic stratus, with the CNT-based parameterizations producing a reservoir that is several orders of magnitude larger than deterministic parameterizations, thereby becoming the dominant factor for sustained strength of ice crystal formation.

In this study we employ a simplistic 1D aerosol-cloud (1D-AC) model informed by observationally-constrained LES results to examine the INP reservoir dynamics of Arctic stratus within a well-mixed cloud-topped boundary layer over sea ice (Knopf et al., 2023b). Our 1D-AC model simulates an evolving vertical column that advects with the mean horizontal wind, thereby approximating a Lagrangian framework to study the INP reservoir in long-lived Arctic clouds. A key simplification of the 1D-AC model is that the liquid phase is taken as a fixed quantity. This approach decouples ice microphysics from liquid-phase feedbacks, enabling a direct attribution of changes in the ice crystal budget solely to the immersion freezing parameterization under investigation (Knopf et al., 2023b). This idealization is physically justified by observations of long-lived Arctic MPCs, which are often characterized by a quasi-steady liquid water path. This state is maintained by very weak ice precipitation rates that only minimally desiccate the cloud, a feature identified in both specific cases (eg., Fridlind et al., 2012) and statistically (eg., Silber et al., 2021). The objective of 1D-AC is to predict the co-evolution of the size- and composition-distributed aerosol acting as INP and the activated N_i profiles in a simplified framework as a function of specified values of the boundary layer turbulent mixing time scale, cloud-top entrainment rate, cloud cooling rate (CCR), and number-weighted ice crystal fall speed (cf. Fridlind et al., 2012). Knopf et al. (2023b) demonstrate how these specified values exhibit markedly differing controls on ice formation depending on which type of ice nucleation scheme is implemented. Different IMF parameterizations derived from the same freezing experiments will scale differently when predicting INPs for conditions other than those of the experiment (Knopf et al., 2021).

Here we extend the Knopf et al. (2023b) study by investigating the impact of different aerosol types and associated PSDs on INPs, IMF parameterizations, and various microphysical and model parameters on the evolution of INP and N_i. To account for the diversity of IMF parameterizations, including the ice nucleation number (INN)-based parameterization (Demott et al., 2010; Demott et al., 2015), INAS parameterization (Niemand et al., 2012; China et al., 2017) and water-activity-based IMF model (ABIFM) parameterization derived from CNT (Knopf and Alpert, 2013; Alpert and Knopf, 2016). We further initialize the model with three different aerosol particle types and respective PSDs, including mineral dust, organic (humic-like substances) aerosol particles, and SSA particles, guided by observations in the Arctic regions. Each of these parameterizations requires different sets of parameter inputs, which will be discussed in detail in the methods section. The effect of varying aerosol number concentration and specified cloud system parameters on the INP reservoir and N_i are also assessed. Furthermore, to assess the model's capability in handling more complex atmospheric compositions and to explore the competitive interplay of different INP types, MPC scenarios incorporating co-existing externally-mixed mineral dust, organic, and sea spray aerosol populations are also investigated. The paper is organized as follows. In Sect. 2 we describe our implementation of the 1D-AC model and all simulation cases in detail. In Sect. 3 we present the sensitivity simulation results, also the findings from combined aerosol scenarios and a detailed INP budget analysis, followed by a discussion in Sect. 4.

https://doi.org/10.5194/egusphere-2025-3620
Preprint. Discussion started: 6 October 2025

Finally, the key findings are summarized and discussed in Sect. 5. Appendix A provides a detailed description of the IMF parameterizations. Appendix B details the INP array calculation in our model for deterministic approaches. The governing equations are presented in Appendix C. For a comprehensive list of symbols and abbreviations, refer to Appendices D and E, respectively.

2 Methods

The 1D-AC model is currently based on cloud system conditions observed in a well-mixed cloud-topped boundary layer over sea ice during the Surface Heat Budget of the Arctic campaign (SHEBA) (Knopf et al., 2023b). In this section, we briefly describe the SHEBA case study. Then we introduce the applied aerosol types and corresponding PSDs and the governing equations of the 1D-AC model. Lastly, we summarize the different simulations considered in this study.

2.1 The SHEBA case study

As the initial setup in our 1D-AC model, we use an Arctic MPC case study that was well observed during the SHEBA campaign (Curry et al., 2000), and that has been widely used for advancing our understanding of MPC conditions (Morrison et al., 2011; Fridlind et al., 2012). The campaign was carried out at roughly 76°N, 165°W in the Beaufort Sea, Arctic Ocean, approximately 570 km northeast of Prudhoe Bay, Alaska. This case study was characterized by widespread, long-lived, shallow MPCs coupled to an underlying pack ice with cloud tops of approximately 600 to 400 m as indicated by Millimeter Wavelength Cloud Radar (MMCR) echoes (Morrison et al., 2011; Fridlind et al., 2012). Rawinsondes provided profiles of temperature and relative humidity (RH), indicating a well-mixed liquid cloud-topped boundary layer. Two-dimensional cloud optical array probes (2D-C), two-dimensional precipitation optical array probes (2D-P) and the Cloud Particle Imager (CPI) yielded reconstructed cloud particle shapes and sizes (Fridlind et al., 2012).

Compared to conditions observed during the Indirect and Semi-Direct Aerosol Campaign (Mcfarquhar et al., 2011) or the Mixed-Phase Arctic Cloud Experiment (Verlinde et al., 2007), this SHEBA case provides a simple starting point owing to ice supersaturated conditions from liquid cloud top to the near-surface as shown in Fig. 1, low liquid water path, high droplet number concentration around 200 cm^{-3}, an absence of liquid-phase precipitation or active ice aggregation, and relatively sparse concentrations of unrimed and nondendritic ice crystals (Fridlind et al., 2018). These conditions are not expected to support secondary ice production (SIP), which is commonly assumed to proceed by rime splintering (Hallett et al., 1974) or freezing fragmentation (Lauber et al., 2018; Keinert et al., 2020), but is currently debated for its relative role in ice production process in MPCs (Phillips et al., 2017; Luke et al., 2021; Waman et al., 2023; Zhao et al., 2023). Robustly observing SIP in both field and laboratory studies is challenging (Korolev et al., 2020b; Silber, 2023), and large uncertainty remains in simulating SIP processes (Phillips et al., 2018; Korolev et al., 2020a; Miltenberger et al., 2021; Burrows et al., 2022; Waman et al., 2023). The apparent occurrence of SIP may be less than 10% in slightly supercooled (warmer than -10°C) Arctic clouds (Luke et al., 2021) and is expected to be negligible under conditions for this SHEBA case (Fridlind et al., 2012) in contrast to other cases

https://doi.org/10.5194/egusphere-2025-3620
Preprint. Discussion started: 6 October 2025

(Fridlind and Ackerman, 2018). Our setup is therefore chosen to isolate the role of primary ice formation via IMF, which precedes any subsequent SIP in non-seeded Arctic stratus.

2.2 Aerosol particle size distributions

To evaluate the impact of different aerosol particle types on the INP reservoir, N_i and ice crystal formation rate, we examine the effects of mineral dust, organic, and SSA particles. During the SHEBA field campaign composition-resolved aerosol PSDs were not measured. Chosen particle types and PSDs, thus, may not represent the ambient aerosol during SHEBA, though all aerosol PSDs are chosen based on measurements performed over Arctic regions. In this sensitivity study, the aim is not having the most realistic representation of the aerosol population for a particular case but to establish if and how different Arctic aerosol types could impact the INP reservoir and N_i. For each aerosol type, the applied aerosol particle size distributions (PSDs) are polydisperse consisting of two or three lognormal modes (Table 1). In addition to Aitken and accumulation modes, this framework includes a larger accumulation mode for aged aerosols and a source-specific SSA mode (Quinn et al., 2017).

Table 1: Summary of the applied particle size distribution parameters for different aerosol types.

Aerosol type	D_1 (μm)	D_2 (μm)	D_3 (μm)	D_{min} (μm)	D_{max} (μm)	σ_1	σ_2	σ_3	N_1^{aer} (cm^{-3})	N_2^{aer} (cm^{-3})	N_3^{aer} (cm^{-3})
Dust	0.20	0.71		0.01	17.32	1.47	2.44		3.47	0.33	
Organic	0.20	0.71		0.01	17.32	1.47	2.44		55.20	0.50	
SSA	0.04	0.17	0.24	0.0022	5.64	1.60	1.55	2.35	38.48	119.70	12.83

The mineral dust and organic PSDs are based on aerosol samples measured by aircraft for single-layer stratocumulus with below-cloud aerosol concentrations less than 250 cm^{-3} (clean cases) as reported in Earle et al. (2011). We use the same lognormal distribution parameters (geometric mean diameter (D), geometric standard deviation (σ)) for mineral dust and organic particles as provided by Savre and Ekman (2015). The aerosol number concentrations for each mode of mineral dust and organic aerosol particles are derived from micro-spectroscopic single particle analysis of ambient particles that were collected by aircraft (Hiranuma et al., 2013). We average particle types from Flight 30-Substrate 6 (F30-S6) during ISDAC to derive respective particle number concentrations. The applied SSA PSD is based on measurements during the International Chemistry Experiment in the Arctic Lower Troposphere (ICEALOT) (Quinn et al., 2017). SSA particles were sampled 18 m above the sea surface. Lastly, to reflect a more realistic aerosol population we combine the mineral dust, organic, and SSA PSD (componsite PSD). Figure 1 displays the lognormal PSDs of the different aerosol particle types and the composite PSD, derived from the modal parameters specified in Table 1.

https://doi.org/10.5194/egusphere-2025-3620
Preprint. Discussion started: 6 October 2025

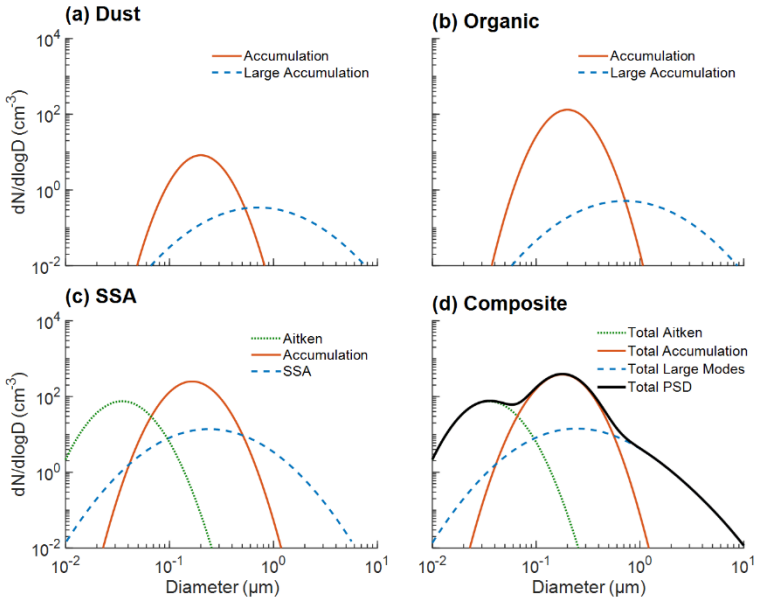

Figure 1: Aerosol particle size distributions for mineral dust (a), organic particles (b), sea spray aerosol (c) and composite particle size distribution (d) following PSD parameters given in Table 1. Different colors represent different modes for respective aerosol PSDs.

2.3 1D-AC model setup

LES baseline results for the SHEBA case study (Fridlind et al., 2012) using the Distributed Hydrodynamic Aerosol and Radiative Modeling Application (DHARMA) code (Ackerman et al., 2000; Stevens et al., 2002) serve as the source of the cloud layer conditions for our model setup. As noted above, 1D-AC maintains a time-invariant thermodynamic profile, including temperature, relative humidity, and liquid water path. We set the domain height to 390 m with the mixed phase cloud layer located from 262.5 to 390 m determined by thermodynamic conditions obtained from SHEBA LES simulation results (see Figure 2). The temperature decreases roughly linearly with height from -16.2 to -19.8 ℃. In this cloud case, the ice supersaturation ratio is larger than 1 throughout nearly the entire domain (see Figure 2), so ice sublimation of sedimenting ice crystals is negligible. The governing model baseline parameter values of mixing time scale, entrainment rate, number-weighted ice fall speed, simulation time step, and simulation vertical resolution applied in the model are shown in Table 2. IMF parameterizations for respective aerosols are summarized in Table 3 and a detailed description of these three IMF parameterizations is given in Appendix A. Above liquid cloud base, all INPs are assumed to be within liquid cloud droplets. To evaluate freezing at subsaturated conditions, i.e., at RH > 90% in this case (i.e., proceeding from a layer just below the cloud base), assuming the INP is engulfed by an aqueous solution below cloud base, we also include a fourth variation, termed ABIFM*, which permits nucleation to occur in subsaturated conditions (Knopf and Alpert, 2013). The calculation of INP arrays for application of the deterministic freezing parameterizations can be found in Appendix B. Prognostic treatments are used for the number concentrations of activatable INPs (the reservoir of INP that can actually be activated within a given cloud

https://doi.org/10.5194/egusphere-2025-3620
Preprint. Discussion started: 6 October 2025

layer, refer to N_{INP}) and N_{i} and detailed prognostic equations are given in Appendix C. The stability of our simulation calculation is evaluated by insuring that results are insensitive to a doubling of vertical resolution (5 m) and a much shorter time step (1 s) (Figure S1). The model framework allows for the simultaneous tracking of multiple aerosol types, each with distinct PSDs and ice nucleation properties, facilitating the External simulations described in Section 2.5. Furthermore, the prognostic equations (Appendix C) enable the diagnosis of individual budget terms for INP number concentration, facilitating the process-level analysis.

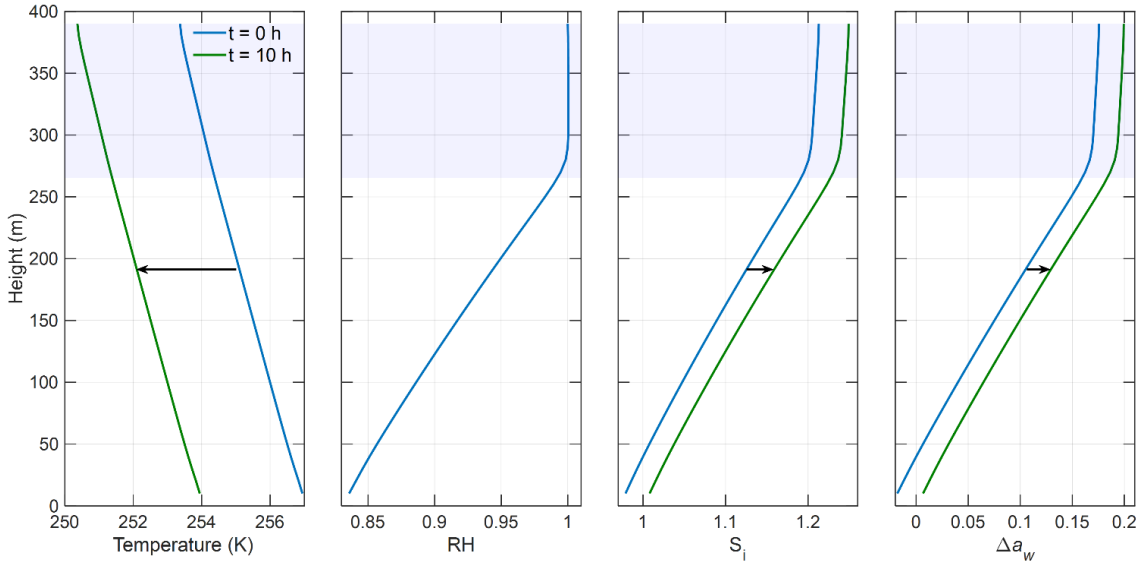

Figure 2: Thermodynamic conditions applied in the minimalistic 1D aerosol-cloud model. From left to right: The temperature (*T*), the relative humidity (RH), supersaturation with respect to the ice (S_{ice}) and Δa_{w}. Blue and green lines represent the initial (t = 0 h) thermodynamic conditions and the thermodynamic conditions with cloud cooling rate of 0.3 °C h^{-1} after 10 h, respectively. The blue shaded area denotes the cloud layer.

Table 2: 1D aerosol-cloud model baseline parameters.

Model parameters	Control run values
Mixing time scale, τ_{mix}	1800 s
Entrainment rate, w_{e}	0.1 cm s^{-1}
Sedimentation rate, v_{f}	30 cm s^{-1}
Simulation time step, δt	10 s
Simulation resolution (vertical), δz	10 m

https://doi.org/10.5194/egusphere-2025-3620
Preprint. Discussion started: 6 October 2025

Table 3: Immersion freezing parameterizations used in this study. Input parameters are aerosol number concentration for particles larger than 0.5 µm, $N_{aer>0.5\mu m}$, aerosol number concentration, N_{aer}, aerosol surface area, A_{aer}, temperature, T, and relative humidity, RH. INP array stores the number concentration of activatable INPs using different data structures for different immersion freezing parameterizations. The INP array dimensions include z_i, height at grid cell index i, t, time, d, INP diameter array, T, INP temperature array.

Immersion freezing parameterizations	Reference	Types of parameterization	Aerosol type	Input	INP array
D2010	*DeMott et al.*, 2010, Eq. 1	Deterministic (INN)	Organic, SSA	$N_{aer>0.5\mu m}, T$	z_i, t, T
D2015	*DeMott et al.*, 2015, Eq. 2	Deterministic (INN)	Mineral dust	$N_{aer>0.5\mu m}, T$	z_i, t, T
N2012	*Niemand et al.*, 2012, Eq. 5	Deterministic (INAS)	Mineral dust	N_{aer}, A_{aer}, T	z_i, t, d, T
C2017	*China et al.*, 2017, Fig. 4b	Deterministic (INAS)	Organic	$N_{aer}, A_{aer}, T,$ RH	z_i, t, d, T
A2022	*Alpert et al.*, 2022, Fig. 5a	Deterministic (INAS)	SSA	$N_{aer}, A_{aer}, T,$ RH	z_i, t, d, T
ABIFM	*Alpert and Knopf*, 2016, Table 2; *China et al.*, 2017, Fig. 4b; *Alpert et al.*, 2022 Fig. 5a	CNT (ABIFM)	Mineral dust, Organic and SSA	$N_{aer}, A_{aer}, T,$ RH	-

2.4 Sensitivity case studies

We investigate the sensitivity of N_{INP}, N_i and ice crystal formation rate (dN_i/dt) with respect to three immersion parameterizations and several key cloud parameters. A key distinction between the schemes, which governs their fundamentally different behaviors, is the realtionship of the INP reservoir (N_{INP}) to the total aerosol population in its composition class (N_{aer}). For instance, mineral dust, a canonical INP class, is highly efficient at nucleating ice but often represents a numerically negligible fraction of N_{aer} compared to more abundant types like organics or sea spray aerosol. In deterministic schemes, N_{INP} represents a limited subset of N_{aer} that are in a composition class based on the temperature at which they may be activated. In contrast, for the CNT-based schemes, all aerosol particles in an INP composition class are treated as potential INPs, making the INP reservoir effectively equivalent to the total aerosol population in that composition class, N_{aer}. We vary the number concentration of aerosols in each composition class (N_{aer}), cloud cooling rate (CCR), cloud-top entrainment rate (w_e) and ice crystal fall velocity (v_f) while applying three aerosol particle types including mineral dust, organic aerosol, and SSA PSDs.

We examine various simulation setups as given in Table 4. The thermodynamic conditions and cloud parameters from the LES baseline results of the SHEBA case study serve as the control run (hereafter referred to as CTRL) while applying the three different aerosol PSDs. We note that the CTRL setup differs slightly from the one used in our previous study (Knopf et al., 2023b). Detailed information on these modifications can be found in Appendix B.

https://doi.org/10.5194/egusphere-2025-3620
Preprint. Discussion started: 6 October 2025

Table 4: Parameter choices of the different 1D aerosol-cloud model simulation. Imm_CTRL: The CTRL run with the baseline settings for all IMF parameterizations, no perturbations, used as a reference. h_res_t and h_res_z: Simulation applying higher resolution with doubly refined vertical resolution (5 m) and much smaller time step (1 s).

Simulations	Description
Control Run	
Imm_CTRL	With the original settings (see Table 2)
Higher Resolution Tests	
h_res_t	δt = 1 s
h_res_z	δz = 5 m
Sensitivity Tests	
N_{aer} x 10	Increasing / decreasing the N_{aer} (number concentration of aerosols) by a factor of 10
N_{aer} x 01	
CCR = 0.3	Cloud cooling rate (CCR) = 0.3 ℃ h^{-1}
w_{e} = 1.0	Entrainment rate (w_{e}) = 1.0 cm s^{-1}
NO_ENTRAIN	Entrainment rate (w_{e}) = 0 cm s^{-1}
v_{f} = 1.0	Ice crystal fall velocity (v_{f}) = 1.0 m s^{-1}
External	External mixture of mineral dust, organic, and SSA particles

To examine the sensitivity of cloud properties (N_{INP}, N_{i} and dN_{i}/dt) towards the parameters N_{aer}, CCR, w_{e} and v_{f}, a series of simulations for each IMF parameterization are carried out by repeating the CTRL case with adjusting the targeted parameters (see Table 4). A detailed summary of all simulations is included in Table 5.

Table 5: Summary of 1D-AC model simulations.

Case	Name	IMF parameterization applied (INN, INAS and ABIFM, respectively)	Description of simulation setup	Number of simulated cases
1	$\mathrm{Imm}_{\mathrm{MD}}^{\mathrm{CTRL}}$	D2015, N2012, ABIFM_dust	Baseline settings for all IMF parameterizations, no perturbations, the CTRL run, used as a reference.	4 (IMF parameterizations) x 3 (particle types): 12
2	$\mathrm{Imm}_{\mathrm{Org}}^{\mathrm{CTRL}}$	D2010, C2017, ABIFM_organics		
3	$\mathrm{Imm}_{\mathrm{SSA}}^{\mathrm{CTRL}}$	D2010, A2022, ABIFM_SSA		

https://doi.org/10.5194/egusphere-2025-3620
Preprint. Discussion started: 6 October 2025

4	$\mathrm{Imm}_{\mathrm{MD}}^{N_{\mathrm{aer}}\ \mathrm{x}\ 10}$	Same as num. 1	N_{aer} is increased or decreased by a factor of 10 compared to the CTRL run.	4 (IMF parameterizations) x 6 (particle types): 24
5	$\mathrm{Imm}_{\mathrm{Org}}^{N_{\mathrm{aer}}\ \mathrm{x}\ 10}$	Same as num. 2		
6	$\mathrm{Imm}_{\mathrm{SSA}}^{N_{\mathrm{aer}}\ \mathrm{x}\ 10}$	Same as num. 3		
7	$\mathrm{Imm}_{\mathrm{MD}}^{N_{\mathrm{aer}}\ \mathrm{x}\ 01}$	Same as num. 1		
8	$\mathrm{Imm}_{\mathrm{Org}}^{N_{\mathrm{aer}}\ \mathrm{x}\ 01}$	Same as num. 2		
9	$\mathrm{Imm}_{\mathrm{SSA}}^{N_{\mathrm{aer}}\ \mathrm{x}\ 01}$	Same as num. 3		
10	$\mathrm{Imm}_{\mathrm{MD}}^{\mathrm{CCR}\ =\ 0.3}$	Same as num. 1	The temperature profiles are modified to linearly decrease by 3 °C over the 10 h simulation.	4 (IMF parameterizations) x 3 (particle types): 12
11	$\mathrm{Imm}_{\mathrm{Org}}^{\mathrm{CCR}\ =\ 0.3}$	Same as num. 2		
12	$\mathrm{Imm}_{\mathrm{SSA}}^{\mathrm{CCR}\ =\ 0.3}$	Same as num. 3		
13	$\mathrm{Imm}_{\mathrm{MD}}^{w_{\mathrm{e}}\ =\ 1.0}$	Same as num. 1	w_{e} is increased from 0.1 cm s^{-1} to 1.0 cm s^{-1} compared to the CTRL runs.	4 (IMF parameterizations) x 3 (particle types): 12
14	$\mathrm{Imm}_{\mathrm{Org}}^{w_{\mathrm{e}}\ =\ 1.0}$	Same as num. 2		
15	$\mathrm{Imm}_{\mathrm{SSA}}^{w_{\mathrm{e}}\ =\ 1.0}$	Same as num. 3		
16	$\mathrm{Imm}_{\mathrm{MD}}^{w_{\mathrm{e}}\ =\ 0}$	Same as num. 1	w_{e} is switched off compared to the CTRL runs.	4 (IMF parameterizations) x 1 (particle types): 4
17	$\mathrm{Imm}_{\mathrm{MD}}^{v_{\mathrm{f}}\ =\ 1.0}$	Same as num. 1	v_{f} is increased from 0.3 m s^{-1} to 1.0 m s^{-1} compared to the CTRL runs.	4 (IMF parameterizations) x 3 (particle types): 12
18	$\mathrm{Imm}_{\mathrm{Org}}^{v_{\mathrm{f}}\ =\ 1.0}$	Same as num. 2		
19	$\mathrm{Imm}_{\mathrm{SSA}}^{v_{\mathrm{f}}\ =\ 1.0}$	Same as num. 3		
20	Imm_External	Same as num. 1, 2, 3	External mixture of mineral dust, organic, and SSA particles each assigned a unique, observationally-based particle size distribution	3 (IMF parameterizations): 3

We multiply the N_{aer} by a factor of 10 and 10^{-1} for CTRL termed experiments N_{aer} x 10 and N_{aer} x 01, respectively. A total of 36 cases are obtained, exploring three different aerosol PSDs (mineral dust, organic and SSA particles), four different IMF freezing parameterizations (INN, INAS, ABIFM and ABIFM*) and three sets of experiments (CTRL, N_{aer} x 10, N_{aer} x 01) (see Table 5).

In order to assess the sensitivity of cloud properties to CCR changes, the temperature profiles for CTRL are modified by applying a cooling rate of 0.3 °C h^{-1} to each layer (see Figure S2). This means that after 10 hours, the entire layer is 3 °C cooler than at the start of the simulation, termed experiment CCR = 0.3 (see Table 4). This results in 24 cases consisting of three aerosol PSDs, four freezing parameterizations and two sets of cases (CTRL for deterministic IMF parameterizations and CNT-based IMF parameterizations and CCR = 0.3) (see Table 5). The evolution of the temperature profiles for CTRL, and CCR = 0.3 are presented in Fig. S2.

https://doi.org/10.5194/egusphere-2025-3620
Preprint. Discussion started: 6 October 2025

Additionally, we investigate the responses of the INPs and N_i evolution to changes in w_e by repeating the CTRL cases while increasing w_e from 0.1 to 1.0 cm s^{-1}, termed experiments w_e = 1.0 which contain 24 cases including three aerosol PSDs, four IMF freezing parameterizations and two sets of experiments (CTRL, w_e = 1.0) (see Table 5).

Lastly, the response of INPs and N_i to changes in v_f is evaluated by changing the v_f from 0.3 to 1.0 m s^{-1}, termed experiments v_f = 1.0 containing 24 cases in total, consisting of three aerosol PSDs, four IMF parameterizations, and two sets of experiments (CTRL, v_f = 1.0) (see Table 5).

2.5 Prognostic Evaluation of IMF Parameterizations in the Presence of Different Aerosol PSDs

To move beyond idealized, single aerosol type studies and demonstrate the model's capability to simulate aerosol populations more representative of the Arctic atmosphere, we conduct simulations representing an external mixture of mineral dust, organic, and SSA particles each assigned a unique, observationally-based particle size distribution (Table 1) (Riemer et al., 2019). We term this simulation as "External". This approach ensures that particles from different sources are treated as physically separate entities while coexisting in the same simulation. The primary goal is to prognostically evaluate how competing aerosol types and associated IMF parameterizations impact N_{INP} and N_i, with freezing initiated by either INN, INAS, or ABIFM as described in Appendix A.

3 Results

3.1 Influence of Immersion Freezing Parameterization on INP and Ice Crystal Evolution

The choice of IMF parameterization fundamentally dictates the simulated temporal evolution of N_{INP}, N_i, dN_i/dt. Figure 3 illustrates the 10-hour domain-averaged time series of N_{INP} for control (CTRL) simulations under different IMF schemes and aerosol types, with Figure S3, S4, S5 providing a detailed view of the initial 0.1 hours. The significant differences in predicted INP concentrations when applying different IMF parameterizations to identical particle size distributions are further illustrated in Figure S6, which demonstrates how parameterization choice can lead to orders-of-magnitude variations in INP predictions. For deterministic IMF schemes (INN, INAS), where INP activation is treated as instantaneous once temperature criteria are met, a rapid decrease in N_{INP} is observed, typically by over 90% from initial values within the first hour (Fig. 3, Table 6, and Fig. S3).

https://doi.org/10.5194/egusphere-2025-3620
Preprint. Discussion started: 6 October 2025

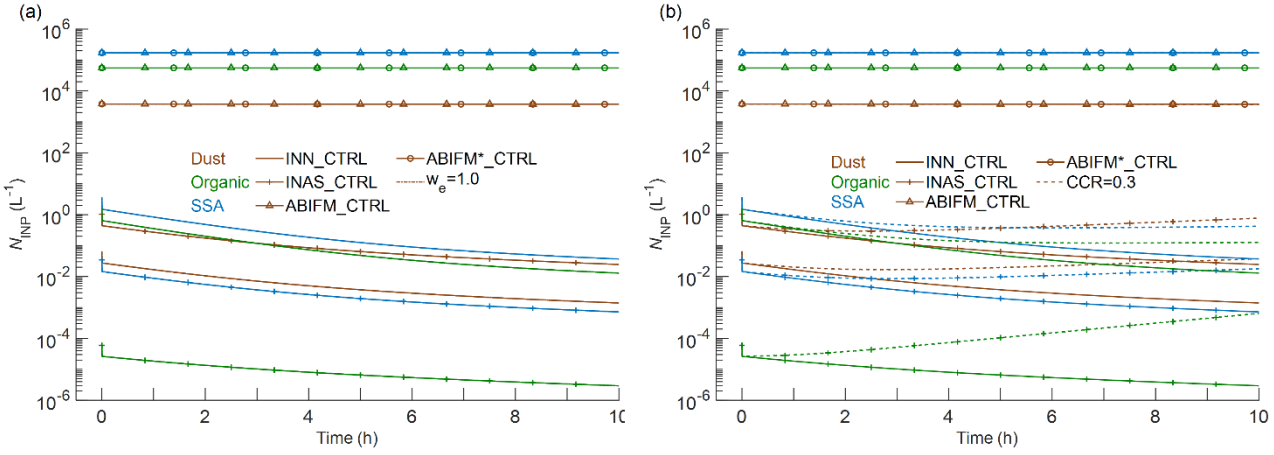

Figure 3. Time series of simulated domain-averaged activatable INP number concentration (N_{INP} in L^{-1}) when changing the cloud-top entrainment rate (a) and cloud cooling rate (b). Simulations are initialized with different aerosol PSDs (dust, organic, and SSA particles), immersion freezing parameterizations (INN, INAS, ABIFM, ABIFM*) and cloud parameters (cloud cooling rate, cloud-top entrainment rate). Brown, green, and blue lines represent the application of aerosol PSDs of dust, organic, and SSA particles, respectively. Simulation results represent different immersion freezing parameterizations: INN (no symbols), INAS (cross), ABIFM (triangle), and ABIFM* (circle). In both panels, the thin solid lines indicate results with the original, unperturbed cloud parameters (CTRL). The dashed lines denote results with the cloud cooling rate (CCR) of 0.3 ℃ h^{-1} (CCR = 0.3) and the dash-dotted lines show the results with the cloud-top entrainment rate (w_e) of 1 cm s^{-1} (w_e = 1.0).

Table 6: The temporal evolution of the domain-averaged number concentration of activatable ice-nucleating particles (N_{INP} in L^{-1}) for given aerosol PSDs (dust, organics and SSA described in Table 1) normalized by the initially activatable INP number concentration, that is $N_{INP}/N_{INP}^{t=0}$, using deterministic ice nucleation number based (INN), the deterministic ice nucleation active sites (INAS), the classical nucleation theory (CNT) water activity based immersion freezing model (ABIFM) and ABIFM enabling subsaturated freezing (ABIFM*). N_{INP} is given for model simulations described in Table 4 for model times 0.5, 5, and 10 h.

	Dust			Organic			SSA		
	0.5h	5h	10h	0.5h	5h	10h	0.5h	5h	10h
INN_CTRL	0.32	0.06	0.02	0.30	0.03	0.01	0.30	0.03	0.01
INAS_CTRL	0.33	0.06	0.02	0.37	0.11	0.05	0.32	0.06	0.02
ABIFM_CTRL	1.00	0.99	0.98	1.00	1.00	1.00	1.00	1.00	1.00
ABIFM*_CTRL	1.00	0.99	0.98	1.00	1.00	1.00	1.00	1.00	1.00
INN_CCR=0.3	0.36	0.30	0.57	0.31	0.08	0.08	0.32	0.10	0.11
INAS_CCR=0.3	0.36	0.35	0.73	0.46	1.77	10.66	0.35	0.28	0.51
ABIFM_CCR=0.3	1.00	0.99	0.97	1.00	1.00	1.00	1.00	1.00	1.00
ABIFM*_CCR=0.3	1.00	0.98	0.97	1.00	1.00	1.00	1.00	1.00	1.00
INN_w_e=1.0	0.32	0.06	0.02	0.30	0.03	0.01	0.30	0.03	0.01
INAS_w_e=1.0	0.33	0.06	0.02	0.37	0.11	0.05	0.32	0.06	0.02
ABIFM_w_e=1.0	1.00	0.99	0.98	1.00	1.00	1.00	1.00	1.00	1.00
ABIFM*_w_e=1.0	1.00	0.99	0.98	1.00	1.00	1.00	1.00	1.00	1.00

https://doi.org/10.5194/egusphere-2025-3620
Preprint. Discussion started: 6 October 2025

This rapid consumption of the initial, limited INP reservoir in deterministic schemes directly impacts ice formation, as shown by the time series of domain-averaged N_i in Figure 4. An initial sharp peak in N_i occurs around 0.2 hours, followed by a substantial decrease. For the CTRL cases, N_i decreases by 86-98% from this peak value after 10 hours.

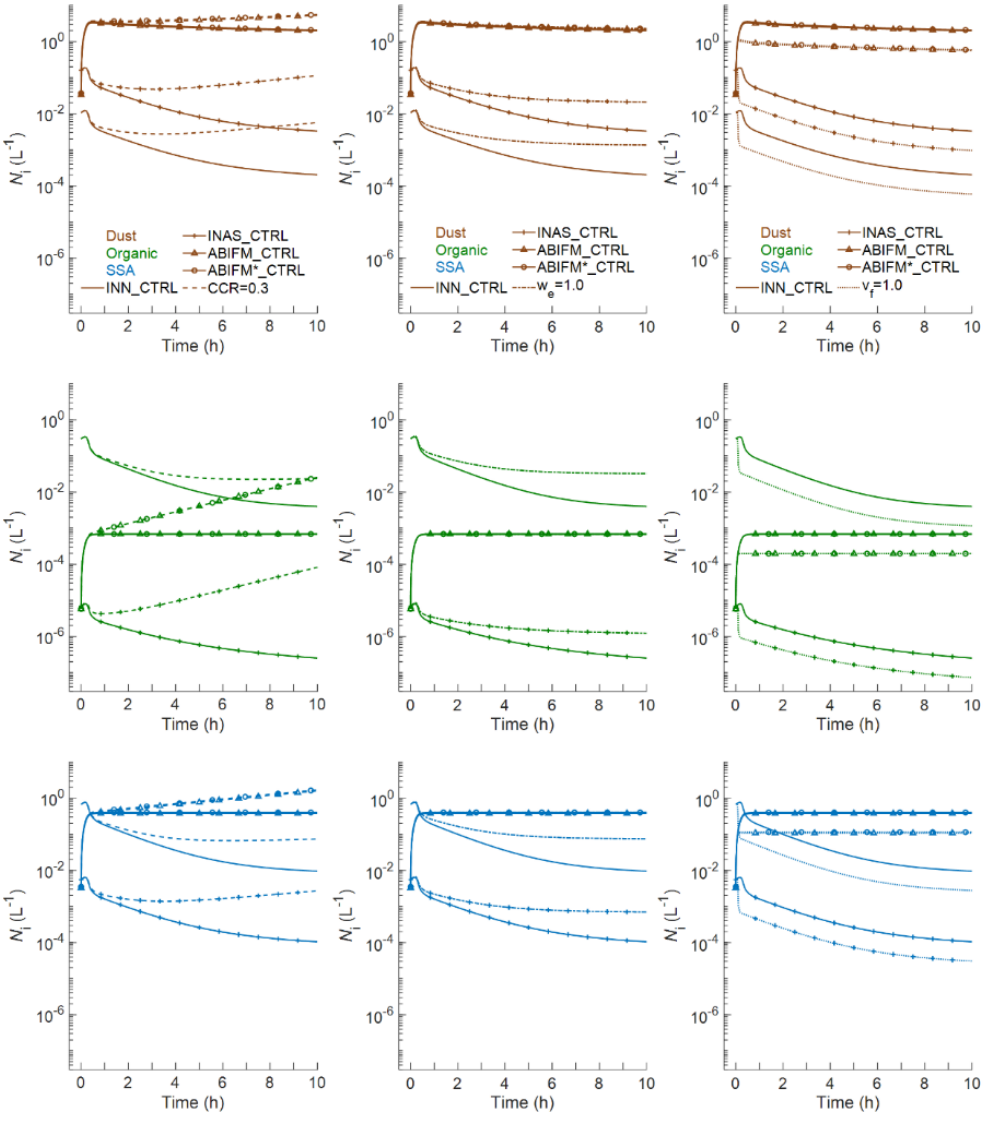

Figure 4: Temporal evolution of the domain-averaged ice crystal number concentration (N_i in L^{-1}) in response to different cloud system parameters. The nine panels are organized by aerosol type in rows (mineral dust, top; organic, middle; and sea spray aerosol (SSA), bottom) and by sensitivity experiment in columns. The columns from left to right represent simulations with an applied cloud cooling rate (CCR), an enhanced entrainment rate (w_e), and an increased ice crystal fall speed (v_f), respectively. Within each panel, different line styles and colors represent the four immersion freezing (IMF) parameterizations, with legends and styling identical to those used in Figure 3.

https://doi.org/10.5194/egusphere-2025-3620
Preprint. Discussion started: 6 October 2025

The dN_i/dt follows a similar trajectory, as depicted in Figure 5. After an initial burst, the formation rate for deterministic schemes decreases by 3-4 orders of magnitude over the 10-hour period, demonstrating the rapid decline in ice production rates following depletion of the initial INP reservoir.

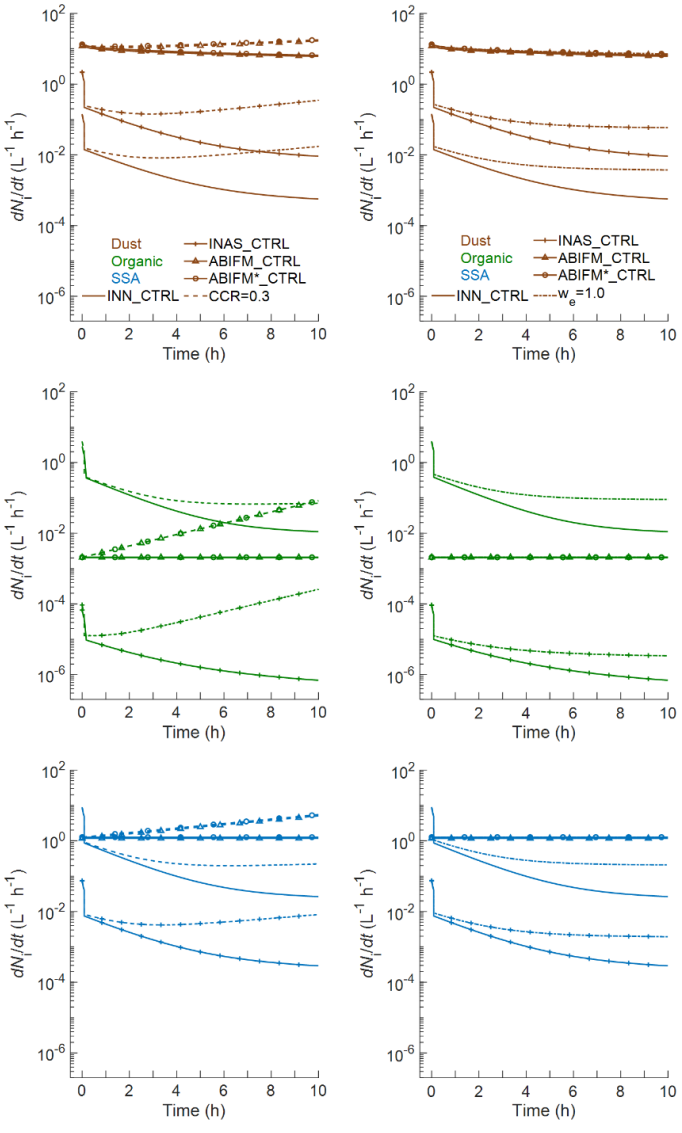

Figure 5: Temporal evolution of the domain-averaged ice crystal formation rate (dN_i/dt in L^{-1} h^{-1}). The six panels are organized by aerosol type in rows (mineral dust, top; organic, middle; and sea spray aerosol (SSA), bottom) and by sensitivity experiment in columns. The columns from left to right show the response to an applied cloud cooling rate (CCR), and enhanced entrainment rate (w_e). Legends and line styles for the four immersion freezing (IMF) parameterizations are identical to those used in Figure 4.

https://doi.org/10.5194/egusphere-2025-3620
Preprint. Discussion started: 6 October 2025

To provide a more quantitative summary of these trends, the evolution of N_i is normalized and presented in Table 7. Unlike N_{INP}, which has a defined value at time zero, N_i only begins to form after the first time step when nucleation processes are activated. Therefore, Table 7 normalizes N_i by its value at the first model output time (t=10 s), providing detailed values that confirm the dramatic decrease observed in the figures.

Table 7: The domain-averaged number concentration of ice crystals (N_i in L^{-1}) normalized by the initial ice crystal number concentraton at the first model output time, that is $N_i/N_i^{t=10\ s}$ following Table 6.

	Dust			Organic			SSA		
	0.5h	5h	10h	0.5h	5h	10h	0.5h	5h	10h
INN_CTRL	0.44	0.05	0.02	0.42	0.03	0.01	0.43	0.04	0.01
INAS_CTRL	0.45	0.05	0.02	0.50	0.09	0.04	0.45	0.05	0.02
ABIFM_CTRL	98.79	71.32	59.39	114.90	118.56	118.56	112.84	116.27	116.25
ABIFM*_CTRL	97.11	68.00	56.21	114.70	118.34	118.34	111.05	114.34	114.32
INN_CCR=0.3	0.50	0.28	0.53	0.44	0.08	0.08	0.45	0.10	0.11
INAS_CCR=0.3	0.52	0.34	0.71	0.69	1.98	12.10	0.51	0.27	0.49
ABIFM_CCR=0.3	102.68	117.95	159.11	129.92	709.88	4422.28	118.52	237.06	490.69
ABIFM*_CCR=0.3	100.98	112.55	150.87	129.70	708.67	4415.27	116.67	233.29	483.03
INN_w_e=1.0	0.55	0.16	0.13	0.51	0.13	0.11	0.52	0.13	0.11
INAS_w_e=1.0	0.56	0.16	0.13	0.64	0.23	0.18	0.55	0.15	0.13
ABIFM_w_e=1.0	99.27	74.94	65.36	114.90	118.56	118.56	112.84	116.28	116.26
ABIFM*_w_e=1.0	97.55	71.54	62.01	114.70	118.34	118.34	111.05	114.35	114.33
INN_v_f=1.0	0.10	0.01	0.01	0.09	0.01	0.00	0.09	0.01	0.00
INAS_v_f=1.0	0.10	0.01	0.01	0.12	0.02	0.01	0.10	0.01	0.01
ABIFM_v_f=1.0	28.08	20.24	16.90	34.07	34.07	34.06	33.24	33.23	33.23
ABIFM*_v_f=1.0	27.45	19.20	15.92	33.99	33.99	33.99	32.57	32.56	32.56

Correspondingly, since ice crystal formation rates are only meaningful after nucleation begins, Table 8 normalizes the dN_i/dt values using the initial rate at t=10 s as the reference. This allows for a clear, quantitative assessment of the rapid decline in ice production rates over the simulation period.

https://doi.org/10.5194/egusphere-2025-3620
Preprint. Discussion started: 6 October 2025

Table 8: The domain-averaged ice crystal formation rate (dN_i/dt in L^{-1} h^{-1}) normalized by the initial ice crystal number concentraton at the first model output time, that is dN_i/dt / $dN_i/dt^{t=10\,s}$ following Table 6.

	Dust			Organic			SSA		
	0.5h	5h	10h	0.5h	5h	10h	0.5h	5h	10h
INN_CTRL	0.00	0.00	0.00	0.00	0.00	0.00	0.00	0.00	0.00
INAS_CTRL	0.00	0.00	0.00	0.00	0.00	0.00	0.00	0.00	0.00
ABIFM_CTRL	0.84	0.61	0.51	1.00	1.00	1.00	1.00	1.00	1.00
ABIFM*_CTRL	0.85	0.59	0.49	1.00	1.00	1.00	1.00	1.00	1.00
INN_CCR=0.3	0.00	0.00	0.00	0.00	0.00	0.00	0.00	0.00	0.00
INAS_CCR=0.3	0.00	0.00	0.01	0.00	0.01	0.09	0.03	0.02	0.03
ABIFM_CCR=0.3	0.89	1.03	1.39	1.20	6.40	39.91	1.08	2.09	4.33
ABIFM*_CCR=0.3	0.90	1.00	1.35	1.20	6.41	39.92	1.08	2.09	4.34
INN_w_e=1.0	0.00	0.00	0.00	0.00	0.00	0.00	0.00	0.00	0.00
INAS_w_e=1.0	0.00	0.00	0.00	0.00	0.00	0.00	0.00	0.00	0.00
ABIFM_w_e=1.0	0.85	0.64	0.56	1.00	1.00	1.00	1.00	1.00	1.00
ABIFM*_w_e=1.0	0.85	0.62	0.54	1.00	1.00	1.00	1.00	1.00	1.00

In contrast, simulations employing CNT-based IMF parameterizations (ABIFM, ABIFM*), where all aerosol particles are potential INPs and activate via a continuous, time dependent freezing process, exhibits a substantially larger and more stable N_{INP} reservoir. N_{INP} remain within ~2% of its initial value at t=0 throughout the 10-hour simulation (Fig. 3a). Table 6 presents these values normalized by their initial value at t=0. Consequently, N_i in CNT-based simulations reach a quasi-stable plateau after an initial increase and remain orders of magnitude higher compared to the case of deterministic schemes (Fig. 4 and Table 7). Similarly, dN_i/dt for CNT schemes is maintained at significantly higher levels (Fig. 5 and Table 8). Simulations with ABIFM* produce domain-averaged N_{INP} and N_i trends broadly similar to the ABIFM cases (Fig. 3 and 4).

3.2 Impact of Aerosol Type and Number Size Distribution

While the choice of parameterization establishes the overarching framework for INP and ice evolution, the specific type and size distribution of aerosol particles further modulate ice nucleation efficiency within these frameworks. The impact of aerosol identity (mineral dust, organic, SSA) on N_{INP}, N_i, and dN_i/dt varies significantly depending on whether INP activation is parameterized based on INN, INAS, or ABIFM.

For the INAS parameterization, which ties ice nucleation to the ice-active site density (n_s) of particles (Eq. A4-A7), aerosol composition is paramount. Despite mineral dust having the lowest total aerosol number concentration (N_{aer}) among the considered types (Table 1), it consistently yields the highest N_{INP} and subsequently N_i and dN_i/dt in CTRL simulations (see Figs. 3, 4, 5, green lines vs. black/blue for INAS crosses). This is directly attributable to the significantly higher n_s values prescribed for mineral dust compared to organic and SSA particles at the relevant cloud temperatures (e.g., Eq. A5 vs. Eqs. A6 and A7). Conversely, for the INN parameterization, which primarily depends on the number concentration of aerosol

https://doi.org/10.5194/egusphere-2025-3620
Preprint. Discussion started: 6 October 2025

particles larger than 0.5 µm (N_{aer} > 0.5 µm, Eqs. A1-A2), the aerosol type itself (beyond its contribution to N_{aer} > 0.5 µm) plays a lesser role. Consequently, SSA, with the highest N_{aer} > 0.5 µm in our PSDs (Table 1), results in the largest initial N_{INP} for INN.

Under the CNT-based ABIFM scheme, where all aerosol particles are potential INPs (N_{INP} = N_{aer}), the initial N_{INP} primarily reflects the total aerosol loading of each type. However, the subsequent ice formation rates are governed by the heterogeneous ice nucleation rate coefficient (J_{het}), which is aerosol-specific (Eqs. A10-A12). Mineral dust, with its generally higher J_{het} values, tends to produce more ice crystals and at a faster rate compared to organic or SSA particles for a given N_{aer} and thermodynamic condition (Figs. 4 and 5, ABIFM triangles). Thus, also when applying a time-dependent freezing process, aerosol identity remains a key factor in determining the intensity of ice production. The differing PSDs associated with each aerosol type (Fig. 2 and Table 1) inherently influence these outcomes by determining the total number and surface area of particles available for nucleation, regardless of the parameterization.

Beyond these inherent differences between aerosol types, we test the system's sensitivity by scaling the total aerosol loading by factors of 10 and 0.1. The results (see Fig. S7) show a straightforward, linear response: the concentrations of N_{INP} and N_i, as well as dN_i/dt, scale proportionally with the initial aerosol loading for all parameterizations.

3.3 Sensitivity to Cloud System Parameters

Beyond the intrinsic properties of aerosols and the choice of freezing parameterization, the dynamic and thermodynamic environment of the cloud system—specifically CCR, w_e, and v_f—exerts significant control over the evolution of INPs and ice crystals.

3.3.1 Cloud Cooling Rate (CCR): A Powerful Driver of Ice Production Intensity

Continuous radiative cooling concentrated at cloud top supports turbulent mixing and leads to progressively declining temperatures throughout the cloud domain, which can drive further INP activation by lowering cloud temperatures (Morrison et al., 2011). The impact of an applied CCR of 0.3 °C h^{-1} is most pronounced for deterministic parameterizations (Figs. 3b, 4, and 5). For these parameterizations, cooling increases the number concentration of activatable INP by lowering the ambient temperature to meet the fixed activation thresholds of a progressively larger and colder subset of the total INP population. (Eqs. A1, A4 and Fig. S2). For example, with INAS, the N_{INP} initially declines due to activation as shown in Fig. 3b (lines with cross signs). However, under continuous cooling (Fig. 3b, dashed lines with cross signs), it can recover and even exceed its initial value after several hours, especially for organic aerosols which exhibits high sensitivity of N_{INP} to temperature changes. Table 6 shows that the organic INAS_CCR=0.3 case reaches over 10 times of initial N_{INP} after 10h. This translates to a large increase in N_i (up to a factor of ~300 for organic INAS, see Table 7) and sustains, or even increases, dN_i/dt compared to CTRL runs where N_i rapidly depletes (Figs. 4 and 5).

https://doi.org/10.5194/egusphere-2025-3620
Preprint. Discussion started: 6 October 2025

For CNT-based approaches, the impact of CCR on the already vast N_{INP} reservoir is minimal (see Table 6, N_{INP} changes by < 3% for ABIFM). However, lower temperatures significantly enhance J_{het}, leading to substantially increased N_i (e.g., N_i increases by factors of ~3-4 for ABIFM with CCR, Table 7) and dN_i/dt (Figs. 4 and 5). This highlights that while the potential INP reservoir in CNT schemes is less sensitive to cooling-induced expansion, the actual rate of ice formation remains highly sensitive to temperature.

3.3.2 Cloud-Top Entrainment Rate (w_e): A Critical INP Source for Depletion-Prone Deterministic Schemes

Cloud-top entrainment of free-tropospheric air provides a mechanism for replenishing INPs. In our simulations with instantaneous activation for deterministic schemes, entrained INPs are immediately converted to ice crystals. Therefore, while the standing N_{INP} concentration within the cloud layer does not show a sustained increase due to entrainment (Fig. 3a, deterministic cases, w_e= 1.0 cm s^{-1} vs. CTRL), this process acts as a continuous source flux (S_{ent}, Fig. 10) sustaining ice production. This is evident in the significantly higher N_i and dN_i/dt observed in deterministic scheme simulations with enhanced entrainment (w_e = 1.0 cm s^{-1}) compared to CTRL runs, particularly after the initial in-cloud INP reservoir is depleted (Figs. 4 and 5). For instance, N_i for INAS with w_e= 1.0 cm s^{-1} can be 3-7 times higher than CTRL after 10 hours (see Table 7, comparing w_e=1.0 to CTRL for INAS).

For CNT-based approaches, entrainment directly adds to the total aerosol particle population (N_{aer}), which constitutes the N_{INP} reservoir. However, minor effects of entrainment can be found. The impact on N_i and dN_i/dt, while positive, is less significant in relative terms compared to deterministic schemes (e.g., N_i increases by ~2-3% for ABIFM with w_e = 1.0 cm s^{-1} after 10 h, Table 7), as the initial reservoir is already substantial and not the primary limiting factor for ice production.

3.3.3 Ice Crystal Fall Speed (v_f): The Primary Sink for Ice Crystals

Ice crystal sedimentation is the sole loss mechanism for ice crystals in our 1D-AC model. Increasing the number-weighted ice fall speed (v_f) from 0.3 m s^{-1} (CTRL) to 1.0 m s^{-1} leads to a more rapid removal of ice crystals from the cloud layer. This results in substantially lower N_i across all parameterizations and aerosol types (Fig. 5). For deterministic schemes, the initial peak in N_i is sharper and the subsequent decline more pronounced, with N_i being roughly an order of magnitude lower after 10 hours with v_f = 1.0 m s^{-1} compared to CTRL (Table 7). Similarly, for CNT-based approaches, higher v_f leads to an approximate 70% reduction in N_i after 10 hours (Table 7). The efficiency of sedimentation thus plays a crucial role in modulating the standing N_i and the lifetime of ice within the mixed-phase cloud.

3.4 Vertical Profiles Reveal Contrasting Sensitivities

While domain-averaged properties provide a valuable overview of the cloud system's response, they can obscure critical height-dependent processes that govern cloud evolution. To deconstruct these mechanisms, we now analyze the vertical profiles of the time-averaged change in INP number concentration ($\Delta N_{INP}(z)$), ice crystal number concentration ($\Delta N_i(z)$), and

https://doi.org/10.5194/egusphere-2025-3620
Preprint. Discussion started: 6 October 2025

ice crystal formation rate ($\Delta dN_i/dt(z)$) in response to changes in CCR, w_e, and v_f. This approach allows us to pinpoint where in the cloud these forcings have their greatest impact and how that impact differs between IMF parameterizations.

3.4.1 INP Concentration Response ($\Delta N_{INP}(z)$)

Figure 6 reveals that the INP reservoir responds in fundamentally different ways to cloud cooling and cloud-top entrainment. For the deterministic INN and INAS schemes, CCR acts as a powerful volume-wide forcing, increasing N_{INP} to values up to ~ 4.6 and ~ 21.4 times the original, respectively, primarily in the upper half of the cloud (Fig. 6a, b). In contrast, the impact of entrainment is sharply localized to the cloud top, providing a boundary-driven source that boosts N_{INP} by up to more than four times its original value. The CNT-based ABIFM scheme shows a different behavior: its large INP reservoir is virtually insensitive to both cooling and entrainment, with ΔN_{INP} remaining less than 1% throughout the vertical column (Fig. 6c, d).

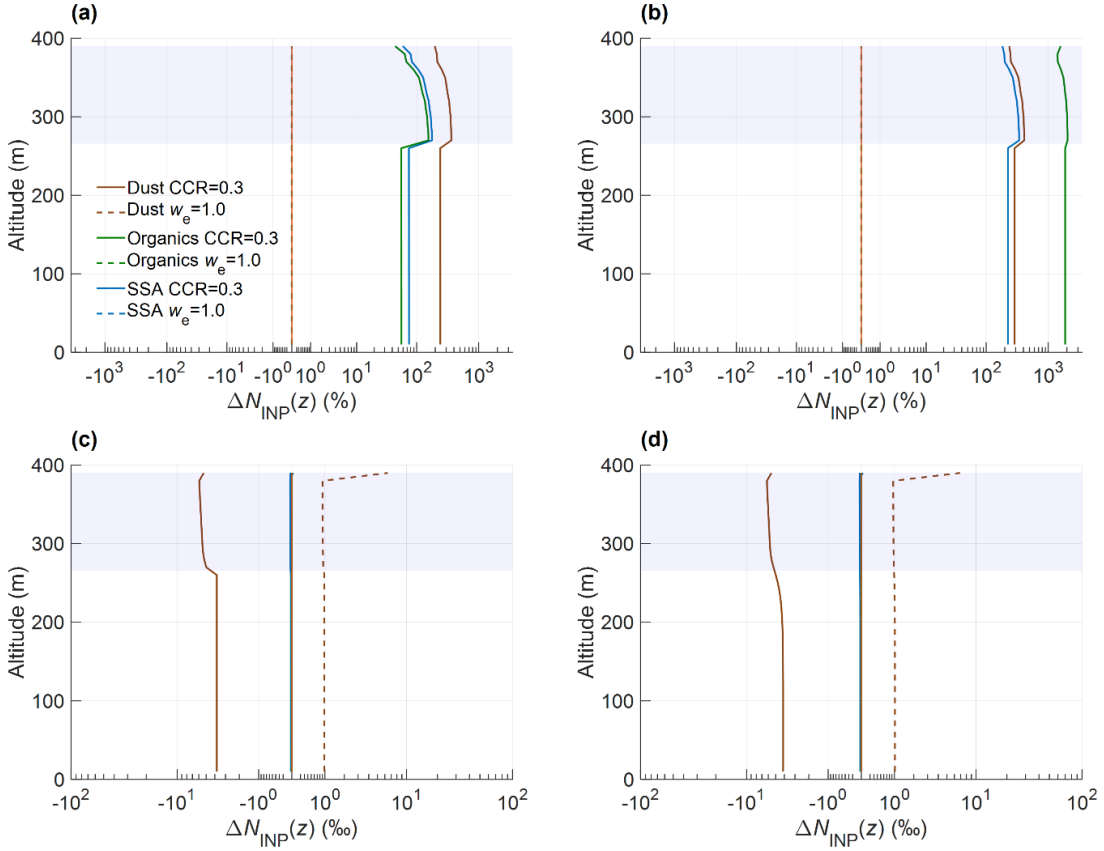

Figure 6: Vertical profiles of the change in number concentration of activatable INP ($\Delta N_{INP}(z)$ in % or ‰) averaged over entire 10 h of simulation time. ΔN_{INP} differs compared to the respective CTRL runs due to the change of cloud parameters (cloud cooling rate, cloud-top entrainment rate) applying dust, organic and SSA particles, given as black, green, and blue lines, respectively. Different immersion freezing parameterizations are applied including (a) ice nucleation number based (INN), (b) ice-nucleation active sites (INAS), (c) water-activity based immersion freezing model (ABIFM), and (d) ABIFM enabling subsaturated freezing (d) ABIFM*. Simulation results for changing cloud cooling rate (solid lines) and cloud-top entrainment rate (dashed lines) are shown. The blue shaded area denotes the cloud layer and the red line in the middle highlights the value of 0.

https://doi.org/10.5194/egusphere-2025-3620
Preprint. Discussion started: 6 October 2025

3.4.2 Ice Crystal Concentration Response ($\Delta N_i(z)$)

The response of the ice crystal concentration ($\Delta N_i(z)$), shown in Figure 7, directly reflects these differing sensitivities. For the INAS scheme, CCR is the dominant factor, driving an enormous $\Delta N_i(z)$ of up to 20-fold (Fig. 7b). The ABIFM scheme is similarly dominated by cooling, which yields a $\Delta N_i(z)$ of up to tenfold (Fig. 7c). Conversely, the INN scheme is more sensitive to entrainment, which causes a nearly five-fold increase in N_i at the cloud top (Fig. 7a). Increasing the v_f acts as a powerful, universal sink. This leads to a substantial negative change in N_i across all parameterizations. As illustrated in Fig. 7 dotted lines, increasing the fall velocity reduces the ice concentration by over 90% throughout the domain.

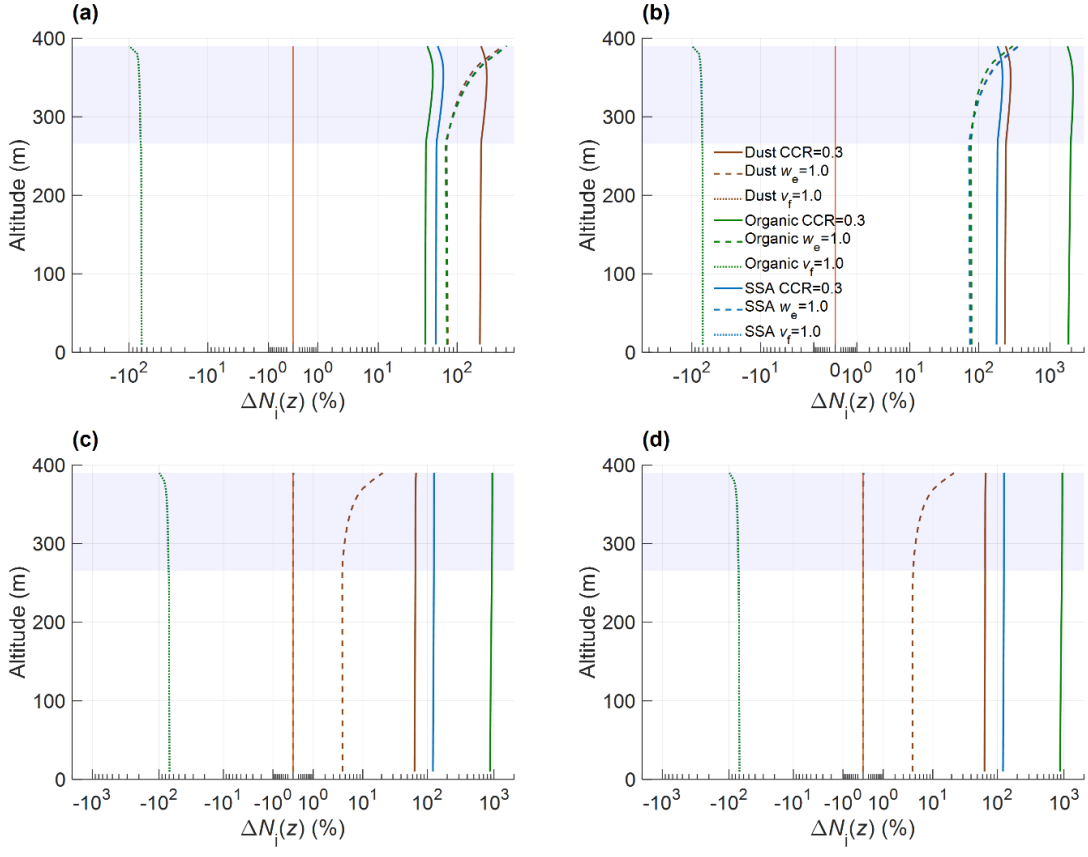

Figure 7: As in Figure 6 but for the change in number concentration of ice crystals ($\Delta N_i(z)$ in %).

3.4.3 Ice Crystal Formation Rate Response ($\Delta dN_i/dt(z)$)

The change in the ice crystal formation rate ($\Delta dN_i/dt(z)$) in Fig. 8 confirms these findings. Cloud cooling enhances the formation rate throughout the entire cloud layer for all parameterizations, with the most dramatic impact seen in the INAS

https://doi.org/10.5194/egusphere-2025-3620
Preprint. Discussion started: 6 October 2025

scheme, where the formation rate shows a peak increase over 25-fold near the cloud top (Fig. 8b). The effect of enhancing cloud-top entrainment is, again, almost exclusively a cloud-top phenomenon. It provides a significant boost to the formation rate for the deterministic schemes (increasing it more than fivefold for INN) but has a minor effect on the CNT-based scheme.

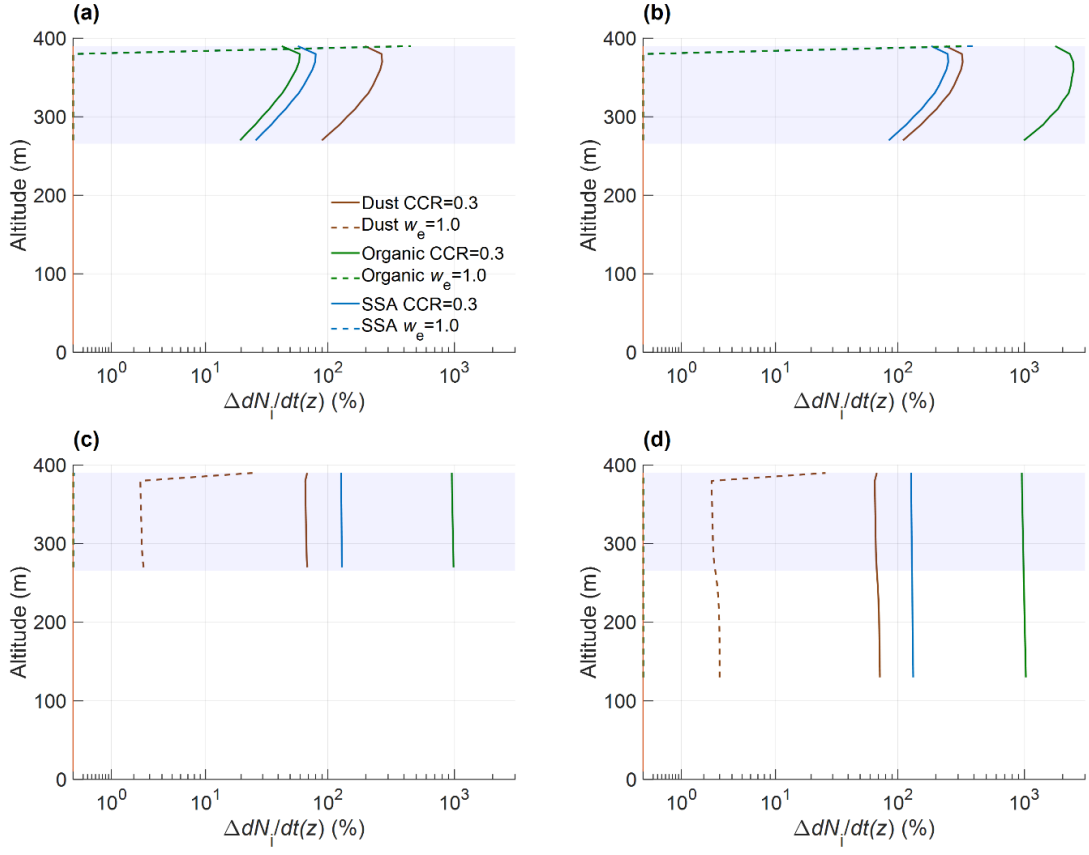

Figure 8: As in Figure 6 but for the change in ice crystal formation rate ($\Delta dN_i/dt(z)$).

3.5 Competing Aerosol in Cloud Ice Formation

The 1D-AC model is configured to simulate a more realistic scenario where mineral dust, organic, and SSA populations coexist, each with their distinct PSDs and INP parameterizations (External). This approach allows for an examination of the model's ability to handle aerosol complexity and, more importantly, to investigate the relative contributions and potential dominance of different aerosol types (Fig. 9). The results show that the dominant source of ice can be governed by a combination of aerosol type and chosen freezing parameterization.

https://doi.org/10.5194/egusphere-2025-3620
Preprint. Discussion started: 6 October 2025

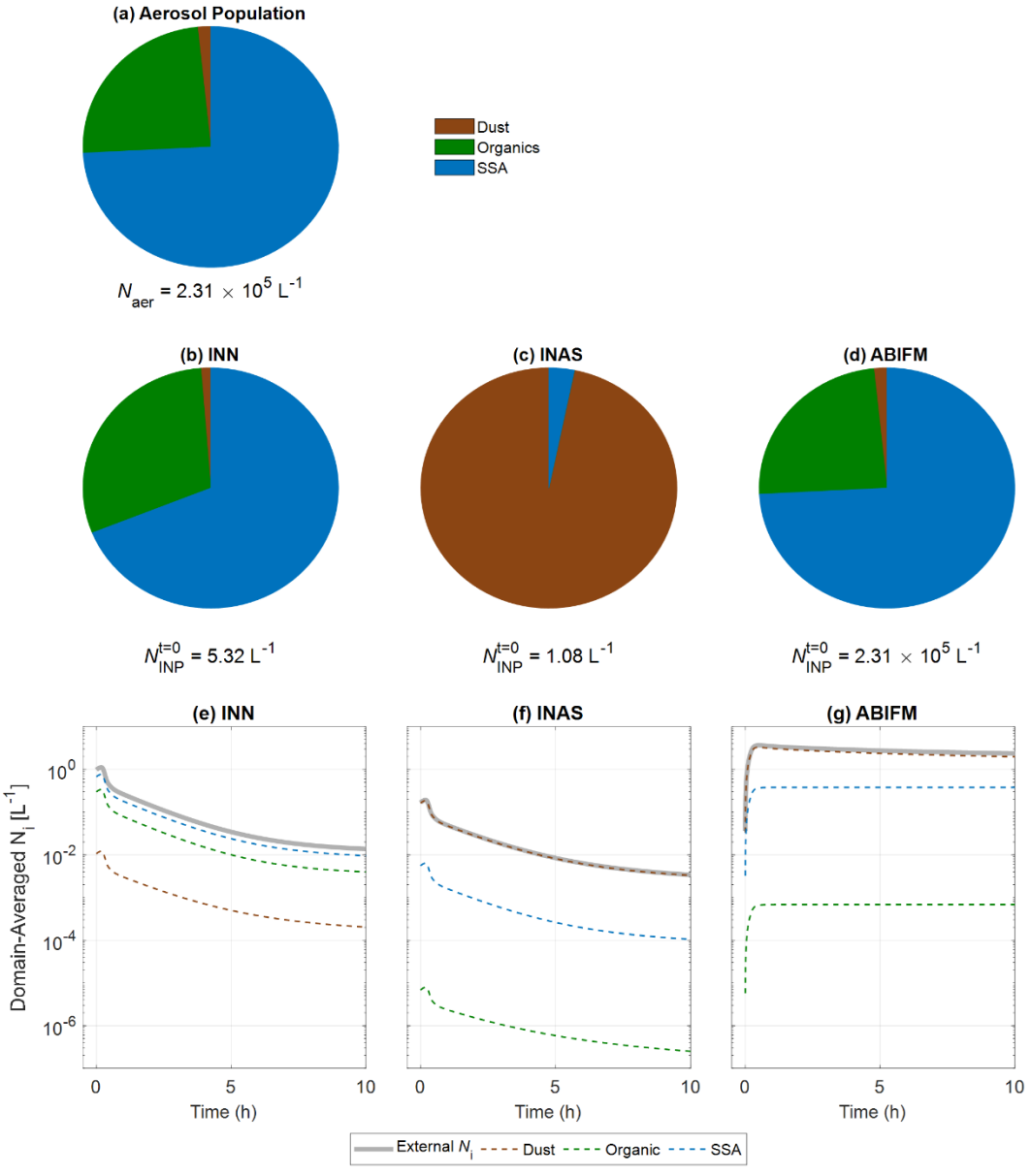

640

Figure 9: Initial total aerosol population, activatable INP composition distribution, and resulting ice crystal number contributions (N_i) using different immersion freezing parameterizations. Panel (a) shows the external aerosol composition. Simulations were run with an aerosol population consisting of dust (brown), organic (green), and SSA (blue) particles. Panels b-d show the initial (t=0) fractional composition of the activatable INP number concentration for each parameterization. Panels e-g show the resulting 645 **domain-averaged N_i over 10 hours and its contribution from each aerosol type. Each column represents a simulation applying INN_External (panels b and e), INAS_External (panels c and f), and ABIFM_External (panels d and g).**

https://doi.org/10.5194/egusphere-2025-3620
Preprint. Discussion started: 6 October 2025

Figure 9a shows the relative contribution of compositionally segregated subpopulations (mineral dust, organic, and sea spray aerosol particles) to the total aerosol number concentration. The aerosol population for these simulations is numerically dominated by organic and SSA particles, which together comprise over 96% of the total particle number concentration. Mineral dust, in contrast, is a minor component by number.

The simulation INN_External identifies 5.32 L^{-1} activatable INPs from particles larger than 0.5 μm, with SSA and organic particles comprising >98% of the initial activatable INPs (Fig. 9b). In this case, the INP concentration, determined solely by temperature and aerosol number concentration, is controlled by the most abundant particles throughout the simulation. SSA serves as the primary ice source (Fig. 9e), with the combined ice concentration decreasing by approximately two orders of magnitude over 10 hours, from ~1 to 10^{-2} L^{-1}.

In contrast, the INAS_External produces an initial activatable INP concentration of only 1.08 L^{-1}, composed almost exclusively (>96%) of mineral dust particles (Fig. 9c). Despite dust representing < 2% of the total aerosol population, its n_s exceeds that of organic aerosols and SSA by several orders of magnitude, thereby dominating ice formation. Accordingly, dust particles control the subsequent ice crystal formation (Fig. 9f). The ice crystal population is composed almost entirely of crystals formed on mineral dust, with negligible contribution from the more abundant but less efficient organic and SSA particles.

The ABIFM_External yields the highest activatable INP concentration (2.31×10^5 L^{-1}), equal to the total aerosol population (Figs. 9a and 9d). Ice production under ABIFM exhibits markedly different dynamics. Despite starting with the fewest activatable INPs, dust ultimately emerges as the dominant source of ice crystals during the 10-hour simulation, followed by SSA and then organic particles (Fig. 9g). Ice crystal number concentration reaching ~2.3 L^{-1} after 10 hours. This is two to three orders of magnitude higher than the final concentrations in the deterministic frameworks .

3.6 Dominant Processes in the INP Budget

To quantitatively diagnose the controlling factors of the simulated INP budget, a comparative analysis is performed for the deterministic (INAS) and CNT-based (ABIFM) parameterizations, specifically for the CTRL simulations initialized with the mineral dust aerosol PSD. All budget terms are expressed as domain-averaged rates. The time-averaged budget balances (Fig. 10a, c) provide a concise summary of the relative magnitudes of INP sources (entrainment) and sinks (activation) over the 10-hour simulation, while the corresponding temporal evolution plots (Fig. 10b, d) reveal the dynamic mechanisms responsible for these balances.

For the deterministic (INAS) parameterization, the time-averaged domain-averaged budget (Fig. 10a) shows a net sink, with the activation term ($S_{\mathrm{act}} \approx$ -0.06 L^{-1} h^{-1}) being an order of magnitude larger than the entrainment source ($S_{\mathrm{ent}} \approx 0.005$ L^{-1} h^{-1}). The temporal evolution of S_{ent} and S_{act} (Fig. 3b) reveals the mechanism behind this imbalance: following an initial rapid activation phase that depletes available INPs within the first hour, the system transitions to an entrainment-limited regime. By approximately 2 hours, the entrainment source and activation sink converge to nearly equal magnitudes (~0.03 L^{-1} h^{-1}), establishing a quasi-steady state where ice formation is controlled by the rate at which new INPs are supplied through entrainment.

https://doi.org/10.5194/egusphere-2025-3620
Preprint. Discussion started: 6 October 2025

In stark contrast, the CNT (ABIFM) parameterization exhibits fundamentally different dynamics. The time-averaged budget terms are two orders of magnitude larger, with a massive activation sink (S_{act} ≈ -7.4 L^{-1} h^{-1}) continuously overwhelming the substantial entrainment source (S_{ent} ≈ 0.5 L^{-1} h^{-1}) (Fig. 10c). The temporal evolution (Fig. 10d) demonstrates that this imbalance is established instantaneously and persists throughout the simulation. Unlike the deterministic case, the activation rate never becomes entrainment-limited but instead maintains relatively high values (~7.7 L^{-1} h^{-1}), reflecting the continuous availability of potential INPs from the large aerosol reservoir characteristic of the stochastic freezing approach. If, however, this reservoir were to be significantly depleted (e.g., in an aerosol-poor environment or over much longer timescales), we would expect the activation rate to eventually become source-limited by entrainment, converging in principle with the behavior of the deterministic case.

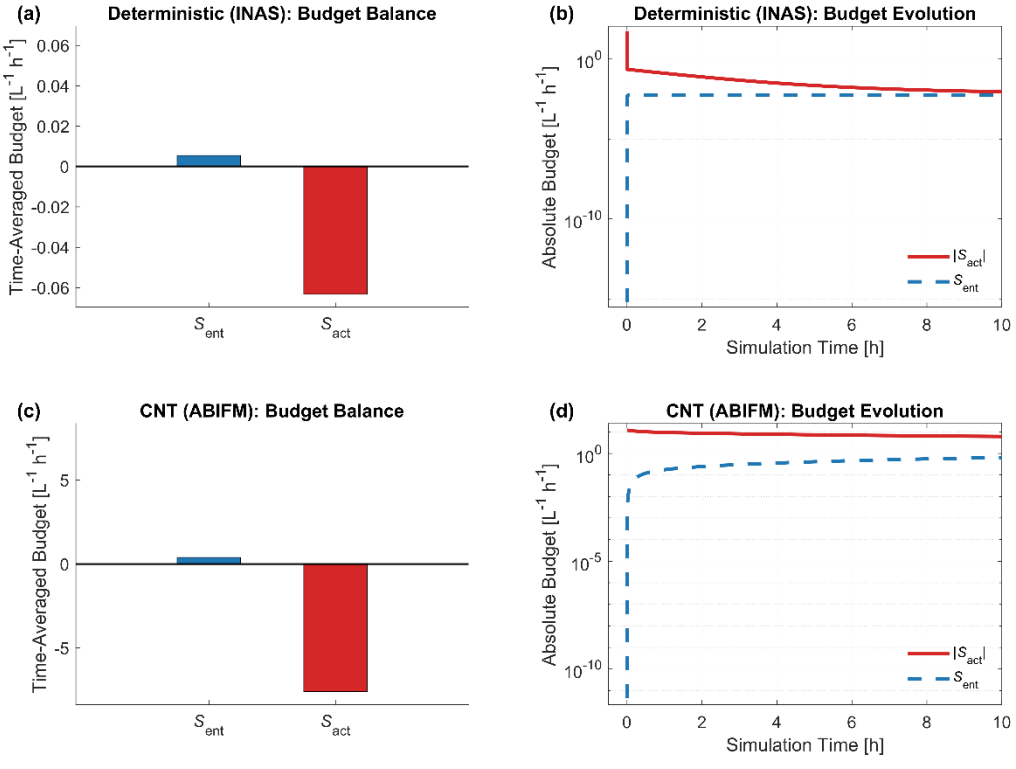

Figure 10: A comparative budget analysis for the control (CTRL) simulation with the mineral dust PSD, illustrating the fundamentally different controls on INP reservoirs applying either deterministic parameterization (INAS) (top row) and the CNT-based parameterization (ABIFM) (bottom row). Panels a and c provide a quantitative summary of the time-averaged domain INP budget balance. Panels b and d reveal the underlying dynamic evolution of the absolute magnitudes of these budget terms over the 10-hour simulation. Note the logarithmic y-axis in panels (b) and (d). All budget terms represent domain-averaged rates in units of L^{-1} h^{-1}.

https://doi.org/10.5194/egusphere-2025-3620
Preprint. Discussion started: 6 October 2025

4 Discussion

4.1 Parameterization Choice Dominates Simulated Ice Phase Evolution

The most striking outcome of this study is the profound impact of the chosen IMF parameterization on the simulated lifecycle of INPs and ice crystals in Arctic mixed-phase stratus over all composition classes and PSDs (Figs. 3, 4, and 5). The orders-of-magnitude difference in the predicted INP reservoir size and N_i between deterministic and CNT-based approaches highlights a fundamental structural uncertainty in representing ice nucleation. Deterministic schemes, by defining INPs as a limited, instantaneously activating subset of aerosols (e.g., Demott et al., 2010; Niemand et al., 2012; Demott et al., 2015), inherently lead to more rapid INP depletion and a more transient ice phase, rendering them highly dependent on continuous replenishment mechanisms. This aligns with previous modeling studies that have shown the necessity of INP replenishment mechanisms to sustain ice in such frameworks (Fridlind et al., 2012; Fridlind and Ackerman, 2018; Knopf et al., 2023b, and references therein).

Conversely, CNT-based approaches, which treat all aerosol particles in their composition class as potential INPs activating continuously over time (e.g., Koop et al., 2000; Knopf and Alpert, 2013, 2023a), maintain a vast INP reservoir. This results in more persistent and significantly higher N_i, suggesting that Arctic MPCs could sustain a more vigorous ice phase if nucleation follows such time-dependent kinetics. The implication is that the perceived need for extremely efficient INP replenishment or additional ice production mechanisms may be reduced if CNT-like processes are dominant. The similarity between ABIFM and ABIFM* results further suggests that, for the simulated conditions, once saturation is achieved, in-cloud nucleation processes appear to be more critical than slow freezing in subsaturated layers below the cloud base for these simulations and conditions.

4.2 Aerosol Characteristics as Modulators of Ice Formation

Within each parameterization framework, aerosol type and PSD further refine ice nucleation predictions. The strong dependence of INAS results on aerosol type (Figs. 3, 4, 5) underscores the importance of accurate n_s parameterizations (Niemand et al., 2012; China et al., 2017; Alpert et al., 2022). The dominance of mineral dust governing N_i, despite lower N_{aer}, is consistent with laboratory findings of its higher n_s values compared to many organic species or SSA at typical MPC temperatures (Hoose et al., 2012a; Kanji et al., 2017). The INN scheme's primary reliance on $N_{aer} > 0.5\mu m$ makes it more sensitive to the aerosol number concentration (Table 1) than to aerosol type differences, a simplification that might not capture the full spectrum of INP behavior (Demott et al., 2010; Knopf et al., 2021). For CNT schemes, while all particles are potential INPs, the aerosol-specific J_{het} values (Alpert and Knopf, 2016) ensure that composition and particle size play a role in determining the rate of ice formation, with dust again often showing higher efficacy.

4.3 Interpretation of Cloud System Parameter Sensitivities

4.3.1 Cloud Cooling and Entrainment: Critical Forcing Mechanisms in Deterministic schemes

https://doi.org/10.5194/egusphere-2025-3620
Preprint. Discussion started: 6 October 2025

The heightened sensitivity of deterministic schemes to CCR and w_e (Figs. 3, 4, and 5; Tables 6 and 7) reinforces their reliance on external drivers to mitigate the rapid depletion of INPs. Our vertical profile analysis (Figs. 6-8) further illustrates these sensitivities by pinpointing how and where different forcings, cloud cooling, cloud-top entrainment impact the cloud properties. These results highlight a fundamental limitation: deterministic schemes cannot sustain ice crystal production on a par with CNT schemes without continuous external forcing, resulting in significant differences in ice production within persistent mixed-phase clouds.

In deterministic schemes, CCR increase the number concentration of activatable INP by lowering temperatures to the activation thresholds of more INPs (Ullrich et al., 2017). This explains the significant increase in ice formation across heights observed in the vertical profiles (Figs. 7 and 8). In contrast, entrainment becomes a direct flux of new INPs that are immediately converted to ice at the cloud top, rather than replenishing a standing INP reservoir. This is why N_{INP} itself (Fig. 3a) shows no direct change with w_e, while N_i is substantially enhanced, leading to a much higher final N_i than in the CTRL run (Table 7), with the increase in N_i sharply localized at the cloud top (Figs. 7 & 8).

CNT-based schemes exhibit markedly different behavior. Due to the immense INP reservoir, their response is governed by nucleation kinetics. Cloud cooling therefore drives a strong, layer-wide increase in ice production by enhancing the nucleation rate, while the minor addition of particles from cloud-top entrainment has a negligible impact on the final ice crystal concentration (Table 7).

The different responses to cloud forcing are a direct consequence of how the INP reservoir is defined. Deterministic schemes, which assume a scarce INP reservoir derived from a subset of aerosols, are critically dependent on cloud cooling and cloud-top entrainment to mitigate their rapid depletion. In contrast, CNT-based schemes, which treat the entire aerosol population as an abundant potential reservoir, are highly responsive to cooling that accelerates freezing but are largely indifferent to the minor perturbation of entrainment. This foundational difference explains why for the deterministic approach, even strong, continuous CCR and cloud-top entrainment can only mitigate depletion, not prevent it - a direct consequence of its initial limited INP reservoir.

4.3.2 Sedimentation Controlling Ice Sink

Sedimentation, controlled by v_f, is the primary removal mechanism for ice crystals across all tested IMF parameterizations (Table 7). Our vertical analysis provides confirmation of this unifying role.

Regardless of the IMF parameterization or the specific forcing applied , the vertical profiles of the change in ice concentration ($\Delta N_i(z)$) consistently show their greatest magnitude—whether positive or negative—in the upper portion of the cloud, with the effect diminishing toward the cloud base (Fig. 7). This robust vertical structure is the clear signature of gravitational removal acting on a distributed, in-cloud source of ice. The highest rates of ice production occur in the coldest, uppermost cloud layers. At the same time, sedimentation continuously removes ice crystals from all levels, transporting them downward.

https://doi.org/10.5194/egusphere-2025-3620
Preprint. Discussion started: 6 October 2025

This interplay between in-cloud ice production and removal creates a natural vertical gradient. The impact of any process perturbation is therefore strongest near the region of most active ice formation and is progressively diminished by sedimentation at lower altitudes.

These results demonstrate that ice crystal fall speed emerges as a critical parameter governing cloud ice distribution, regardless of the specific microphysical processes involved. Consequently, accurate representation of ice particle fall speeds becomes essential in models.

4.4 Competitive Ice Nucleation: Insights from Externally-Mixed Aerosol Simulations

Each IMF parameterization uses different physical assumptions that determine how aerosol particles contribute to the activatable INP population, creating distinct relationships between the initial aerosol population, the activatable INP reservoir, and the resulting N_i.

INN parameterization rely on aerosol number concentration. Since SSA and organic aerosols dominate the number concentration in this size range, they predominantly comprise the initial activatable INP pool (Fig. 9b). Consequently, the resulting ice crystal population reflects this abundance pattern, with SSA serving as the primary contributor to ice formation (Fig. 9e).

In contrast, the INAS parameterization is based on aerosol type and surface area. The freezing efficiency for each aerosol type is described by n_s. For the examined external aerosol, our simulations demonstrate that the n_s term governs the ice nucleation response. This is because, the n_s values for mineral dust exceed those of SSA and organic particles by several orders of magnitude. This substantial difference in intrinsic ice nucleation efficiency enables the relatively sparse dust particles to dominate the activatable INP reservoir (Fig. 9c), despite their lower number concentrations. Accordingly, dust particles control the subsequent ice crystal formation (Fig. 9f).

The CNT-based ABIFM parameterization assumes a time-dependent freezing process. Hence, all aerosol particles serve as potential INPs, such that the initial activatable INP reservoir mirrors the total aerosol number distribution, dominated by SSA and organic particles (Fig. 9c). However, the final N_i is dominated by dust (Fig. 9g). Similar to INAS, this is due to the larger nucleation rate coefficient (J_{het}) of dust compared to SSA and organic particles. Over the 10-hour simulation period, the substantially higher nucleation rates of dust particles enable more rapid ice crystal production, ultimately outcompeting other aerosol types.

This study demonstrates our model's capacity to prognostically evaluate competing ice microphysics parameterizations using realistic aerosol PSDs. By simulating competitive nucleation between multiple aerosol populations, we move beyond single-type sensitivity tests toward conditions that better represent atmospheric complexity. These results address a fundamental question in ice microphysics: Is atmospheric ice formation controlled by rare but highly efficient particles, or by the collective contribution of abundant aerosols? Our modeling framework provides the quantitative tools needed to test these competing paradigms against field observations, ultimately constraining which parameterizations most accurately reproduce observed cloud microphysical properties.

https://doi.org/10.5194/egusphere-2025-3620
Preprint. Discussion started: 6 October 2025

4.5. Process-Level Controls on INP Evolution: A Budget Perspective

The budget analysis reveals contrasting behaviors between the INAS and CNT (ABIFM) parameterizations: although their time-averaged activation-to-entrainment ratios are similarly around~10:1 (Fig. 10a,c), the absolute magnitudes differ by two orders of magnitude, and the temporal evolution diverges markedly (Fig. 10b,d). The deterministic parameterization exemplifies source-limited behavior. Following rapid depletion of the INPs (Fig. 10b), ice production becomes entirely controlled by cloud-top entrainment of INPs. The modest long-term budget balance (Fig. 10a) reflects this supply limitation, where S_{ent} dictates ongoing ice formation, independent of the freezing parameterization.

In contrast, the CNT parameterization exhibits process-rate-limited dynamics. The sustained, high-magnitude activation sink (Fig. 10d) demonstrates nucleation acting on an abundant aerosol reservoir, with S_{act} vastly exceeding S_{ent} (Fig. 10c). Here, ice production is governed by the intrinsic freezing kinetics under ambient thermodynamic conditions, enabling rapid glaciation potential absent in the deterministic framework.

This process-level comparison demonstrates that choice of freezing parameterization represents a selection between fundamentally differnent hypotheses for primary ice formation. The stark differences in baseline dynamics (Fig. 10) underscore how this choice directly impacts simulation results.

5 Summary and Conclusions

The objective of this study is to dissect the key processes and uncertainties that govern ice formation in Arctic mixed-phase clouds. First, we explore structural uncertainty in primary ice formation by evaluating how three different immersion freezing ice nucleation parameterizations influence the microphysical evolution of mixed-phase Arctic stratus in the SHEBA MPC case, using three aerosol types with distinct particle size distributions. Second, we assess the sensitivity of INP reservoir dynamics — specifically N_{INP} and N_{i} — to variations in aerosol number concentration (N_{aer}) and key cloud and atmospheric parameters, including cloud cooling rate (CCR), entrainment velocity (w_{e}), and ice crystal fall speed (v_{f}). Furthermore, we investigate competitive nucleation among different aerosol types in a more realistic scenario using externally-mixed aerosol populations and conduct a detailed INP budget analysis to diagnose and quantify the dominant processes controlling the INP reservoir. We address these objectives using a version of the 1D-AC model extended to include multiple aerosol types and their specific freezing parameterizations, informed by LES of the SHEBA case (Knopf et al., 2023b). The main findings can be briefly summarized as follows.

1. When treating INPs prognostically as done in this study, the choice of IMF parameterizations can yield contrasting concentrations and trends of simulated N_{INP}, N_{i}, and dN_{i}/dt. Compared to deterministic approaches, a time-dependent description (CNT) yields an orders of magnitude larger INP reservoir, a finding consistent with previous work (Knopf et al., 2023b). This leads to ice crystal formation at a substantially higher rate without significant INP depletion , resulting in a simulated ice phase that is more persistent and not limited by the same replenishment fluxes as the deterministic schemes.

https://doi.org/10.5194/egusphere-2025-3620
Preprint. Discussion started: 6 October 2025

2. Different aerosol types and associated PSDs significantly modify the magnitude of the simulated N_{INP}, N_{i}, and dN_{i}/dt but do not alter their trends observed in the control run. The relative roles of aerosol types and associated PSDs are primarily dependent on the choice of IMF parameterizations.
3. Among all microphysical parameters tested, changing the N_{aer} elicits a directly proportional response in the simulated N_{INP}, N_{i}, and dN_{i}/dt across all parameterizations. For example, increasing N_{aer} by a factor of 10 leads to a corresponding ten-fold increase in these variables, and vice-versa.
4. Changing the N_{aer} has a directly proportional impact on N_{INP}, N_{i}, and dN_{i}/dt. In contrast, cloud cooling (CCR), w_{e}, and v_{f} have non-linear effects, with the dominant process for ice production depending on the chosen parameterization. For deterministic approaches, where the INP reservoir is limited, ice production is critically dependent on the w_{e} for replenishment. For CNT-based approaches with an abundant INP reservoir, CCR becomes the dominant control; it can reverse the overall decline in ice crystal concentration and, specifically for organic aerosols, drive N_{i} to levels that substantially exceed the initial peak.
5. Initiating IMF under subsaturated conditions (when using ABIFM) leads to a more gradual trend in vertically resolved cloud properties around the cloud base compared to in-cloud only nucleation. These trends do not significantly impact the conclusions of the cases investigated in this study. However, we cannot fully rule out the potential importance of parameterization choices in accounting for IMF under subsaturated conditions more generally.

The 1D-AC model simulation results support the following conclusions. Our findings underscores the importance of the IMF parameterization selection in modeling mixed-phase Arctic stratus. Although each examined IMF parameterization was derived from laboratory experiments, the significant differences, particularly between deterministic and CNT-based approaches, when simulating N_{INP}, N_{i}, and dN_{i}/dt from aerosol PSDs highlight the profound uncertainty in extrapolating these frameworks to atmospheric conditions and the necessity to constrain them with in-situ observations. Considering that primary ice formation is a ubiquitous phenomenon in Arctic MPCs, characterized by a low liquid water path (Silber et al., 2021), there is an urgent need for more laboratory and field research to better assess the scaling of IMF parameterizations under realistic MPC conditions (Knopf et al., 2020; Knopf et al., 2021; Burrows et al., 2022; Knopf and Alpert, 2023a).

The starkly different model behaviors emerging from these two different freezng parameterizations have significant implications for climate modeling. The CNT framework predicts sustained ice production without the same dependency on strong, continuous replenishment fluxes seen in the deterministic framework. As a consequence, interpretation of the evolution of a mixed-phase cloud including cloud lifetime and radiative properties will be different and will crucially depend on which freezing description is more representative of nature. A separate, practical advantage of the CNT approach is its computational simplicity. CNT-based methods do not require the INP array at all. This simplification removes the necessity of temperature-dependent INP arrays, reducing the complexity of the computational model. By eliminating the need to track additional variables for particle uniqueness, the model becomes more streamlined. Consequently, the time-dependent approach, which

https://doi.org/10.5194/egusphere-2025-3620
Preprint. Discussion started: 6 October 2025

provides freezing rates, enhances the feasibility of incorporating prognostic capabilities into global models with size-resolved aerosol modules (Bauer et al., 2008; Liu et al., 2016).

We evaluated three typical aerosol particle types: mineral dust, organic and SSA. Other potentially significant INP types (such as biological particles or biomass-burning aerosols) could also impact ice formation rates in Arctic MPCs. In future studies, the impact of other atmospheric INPs on cloud glaciation should be investigated. Continued work is needed to develop accurate ice nucleation parameterizations that cover the temperature range of realistic MPC conditions.

The observed non-linear responses of N_{INP}, N_{i}, and dN_{i}/dt to changes in CCR, w_{e}, and v_{f} highlight the importance of detailed cloud microphysical and dynamical measurements. Additional profiling observations of MPC temperatures, number concentration of free-troposphere aerosol particles, and the characterization of ice crystal fall velocity are essential for robustly evaluating the representation of INP reservoirs in mixed-phase Arctic stratus.

https://doi.org/10.5194/egusphere-2025-3620
Preprint. Discussion started: 6 October 2025

APPENDIX A

Immersion freezing parameterizations

The deterministic INN parameterization of mineral dust particles acting as INPs is given by (Demott et al., 2015, D2015)

$$\sum_{T=T_{min}}^{T_{\mathrm{INP}}} N_{\mathrm{INP}}^{\mathrm{sing\ (INN)}}(T) = cf\left(N_{\mathrm{aer}>0.5\mu m}\right)^{1.25} e^{(0.46(-T_{\mathrm{INP}})-11.6)}. \quad \text{(A1)}$$

$N_{\mathrm{INP}}^{\mathrm{sing\ (INN)}}(T)$ is the number concentration of all activatable INPs which are particles can serve as INPs and potentially be activated (hereafter referred to as INPs) at temperature T, cf is the calibration factor with a value of 3 suggested when applying this parameterization to atmospheric data, $N_{\mathrm{aer}>0.5\mu m}$ is the total number of aerosol particles with diameters larger than 0.5 μm, and T is the temperature in the unit of Celsius.

A similar deterministic INN parameterization of ambient aerosol particles acting as INPs is given by (Demott et al., 2010, D2010)

$$\sum_{T=T_{min}}^{T_{\mathrm{INP}}} N_{\mathrm{INP}}^{\mathrm{sing\ (INN)}}(T) = 0.0000594(-T)^{3.33}\left(N_{\mathrm{aer}>0.5\mu m}\right)^{(0.0264(-T_{\mathrm{INP}})+0.0033)}. \quad \text{(A2)}$$

We applied this IMF parameterization (Eq. A2) for the case of SSA and organic particles while noting that this does likely not reflect SSA and organic particles but represents ambient atmospheric particles in general.

In the 1D-AC model, the INN parameterizations are implemented as follows:

$$N_{\mathrm{INP}}^{\mathrm{Imm}}(z_i, t, k_*^{\mathrm{Imm}}) = N_{\mathrm{INP}}^{\mathrm{sing\ (INN)}}(z_i, t, T_{\mathrm{INP}}) H\left(T(z_i, t)\right), \quad \text{(A3)}$$

where $N_{\mathrm{INP}}^{\mathrm{sing\ (INN)}}$ is multiplied by a Heaviside function $H\left(T(z_i, t)\right)$, which equals to 1 when $T(z_i, t) > T_{\mathrm{INP}}$ and 0 otherwise. This function ensures that INP activation occurs only when the temperature is lower than the activation temperature of INPs. In the model configuration used in this study, the array of T_{INP} designates the activation temperature of INPs per temperature bin using geometric progression bins.

The INAS parameterization of natural dust particles acting as immersion INPs is given as (Niemand et al., 2012, N2012):

$$\sum_{T=T_{\mathrm{min}}}^{T_{\mathrm{INP}}} N_{\mathrm{INP}}^{\mathrm{sing\ (INAS)}}(T, d) = N_{\mathrm{aer}}(d)(1 - e^{-A_{\mathrm{aer}}(d) n_{\mathrm{s}}(T_{\mathrm{INP}})}) \quad \text{(A4)}$$

$$n_{\mathrm{s}}{}^{\mathrm{dust}}(T_{\mathrm{INP}}) = e^{(-0.517(-T_{\mathrm{INP}})+8.934)}. \quad \text{(A5)}$$

$N_{\mathrm{INP}}^{\mathrm{sing\ (INAS)}}(T, d)$ is the number concentration of all activatable INPs in temperature bin T and diameter bin d, N_{aer} is the total number concentration of aerosol particles, A_{aer} is the individual particle surface area, n_{s} is the INAS density in units of m^{-2}.

For organic particles (humic-like substances) and SSA, the n_{s} is given by China et al. (2017) (C2017) and (Alpert, 2022) (A2022), respectively, as

$$n_{\mathrm{s}}{}^{\mathrm{organic}}(T_{\mathrm{INP}}) = 10^{(66.90259(\Delta a_{\mathrm{w}})-12.322)} \quad \text{(A6)}$$

$$n_{\mathrm{s}}{}^{\mathrm{SSA}}(T_{\mathrm{INP}}) = 10^{(24.02526(\Delta a_{\mathrm{w}})-2.26105)}, \quad \text{(A7)}$$

https://doi.org/10.5194/egusphere-2025-3620
Preprint. Discussion started: 6 October 2025

where Δa_{w} is the water activity criterion, given below.

In this model, the INAS parameterizations are implemented as follows:

$$N_{\mathrm{INP}}^{\mathrm{Imm}}(z_i, t, k_*^{\mathrm{Imm}}) = N_{\mathrm{INP}}^{\mathrm{sing\ (INAS)}}(z_i, t, d, T_{\mathrm{INP}}) H\big(T(z_i, t)\big)\,. \tag{A8}$$

For the INAS case, the T_{INP} array is set same as in the INN case, while the d array is defined using 50 bins, with a bin to bin mass ratio of 1.5. This implies that each subsequent bin has 1.5 times as much the mass as the previous one.

ABIFM parameterizes the heterogeneous ice nucleation rate coefficient J_{het}, as a function of the water activity criterion, Δa_{w} (Knopf and Alpert, 2013). Derived from the water activity at the ice melting temperature, $a_{\mathrm{w}}^{\mathrm{i}}$, and water activity at the freezing temperature, a_{w}, Δa_{w} is used in ABIFM to describe IMF as a function of ambient T and RH:

$$\Delta a_{\mathrm{w}}(T) = a_{\mathrm{w}}(T) - a_{\mathrm{w}}^{\mathrm{i}}(T). \tag{A9}$$

Notice that, for IMF from water droplets, $a_{\mathrm{w}}(T) = 1$, while under subsaturated conditions, $a_{\mathrm{w}}(T) < 1$. The equation for $a_{\mathrm{w}}^{\mathrm{i}}(T)$ is given in Koop et al. (2009). To evaluate freezing at subsaturated conditions, i.e., at RH > 90%, we conducted additional model simulations termed ABIFM*.

ABIFM and ABIFM* derive J_{het} in units of $\mathrm{cm^{-2}\ s^{-1}}$ for mineral dust, organic particles, and SSA particles in the following way (Alpert and Knopf, 2016; China et al., 2017; Alpert et al., 2022), respectively:

$$\log_{10}\left({J_{\mathrm{het}}}^{\mathrm{dust}}\big(\Delta a_{\mathrm{w}}(T)\big)\right) = 22.62\Delta a_{\mathrm{w}}(T) - 1.35 \tag{A10}$$

$$\log_{10}\left({J_{\mathrm{het}}}^{\mathrm{organic}}\big(\Delta a_{\mathrm{w}}(T)\big)\right) = 66.90259\Delta a_{\mathrm{w}}(T) - 13.40148 \tag{A11}$$

$$\log_{10}\left({J_{\mathrm{het}}}^{\mathrm{SSA}}\big(\Delta a_{\mathrm{w}}(T)\big)\right) = 26.6132\Delta a_{\mathrm{w}}(T) - 3.9346\,. \tag{A12}$$

In the CNT case, the number concentration of activatable INPs, $N_{\mathrm{INP}}^{\mathrm{CNT\ (ABIFM)}}$, is given by

$$N_{\mathrm{INP}}^{\mathrm{CNT\ (ABIFM)}}(d) = N_{\mathrm{aer}}(d)\,, \tag{A13}$$

where $N_{\mathrm{aer}}(d)$ is the number concentration of the applied aerosol particle type per bin.

In the 1D-AC model, the CNT-based IMF parameterizations are implemented as follows:

$$N_{\mathrm{INP}}^{\mathrm{Imm}}(z_i, t, k_*^{\mathrm{Imm}}) = N_{\mathrm{INP}}^{\mathrm{CNT\ (ABIFM)}}(z_i, t, d)\,. \tag{A14}$$

The d array has the same characteristics as for the INAS case.

https://doi.org/10.5194/egusphere-2025-3620
Preprint. Discussion started: 6 October 2025

APPENDIX B

INP array calculation for deterministic approaches

In deterministic approaches, the model employs a decoupled framework that separates the intrinsic INP activation spectrum from its environmental expression. This design ensures consistent initialization across simulations while allowing dynamic evolution based on atmospheric conditions.

Temperature array construction

The temperature array is constructed to ensure finer resolution at lower temperatures, where ice nucleation is more sensitive. This array is generated using a geometric progression, with the temperature bins increasing exponentially. The freezing array begins at a minimum temperature T_{min} = -38 ℃ and the temperature increments are determined by an initial temperature step ΔT_0 (the ΔT between the first and second temperature bin edges) and an exponential factor dT_{exp} (the ratio of ΔT between consecutive bins).

The progression continues, but the array stops when the next temperature value is greater than or equal to the maximum temperature T_{max} = -5 ℃, meaning the last value in the array may not be reached at exactly T_{max}. The temperature array is constructed as:

$$T_{\text{array}} = \left[T_{min}, T_{min} + \Delta T_0, T_{min} + \Delta T_0 \cdot dT_{\text{exp}}^{(1)}, T_{min} + \Delta T_0 \cdot dT_{\text{exp}}^{(2)}, \ldots\right] \text{ while } T < T_{max} \quad \text{(B1)}$$

INP reservoir initialization

Using established parameterizations (Appendix A), the model calculates the cumulative INP concentration active at or below each temperature, then discretizes this into a differential activation spectrum $N_{\text{INP}}(T)$ representing INPs that activate specifically within each temperature bin. This creates the baseline INP reservoir array: $\text{INP}_{\text{array}}(z, T, t)$.

Dynamic evolution and filtering

During simulation, the INP reservoir evolves through entrainment of new INPs from external sources, permanent removal through activation when environmental temperature drops to or below a bin's activation temperature (conversion to ice crystals), and vertical redistribution via mixing without changing total INP numbers.

At each timestep, the model applies a dynamic temperature mask based on the minimum column temperature to determine the potentially activatable INP concentration:

$$\text{INP}_{\text{totarray}}(z, t) = \sum_{T \geq T_{\text{cloud top}}} \text{INP}_{\text{array}}(z, T, t) \quad \text{(B2)}$$

This approach ensures that only INPs with activation temperatures warmer than current conditions remain in the activatable reservoir, while consumed INPs are permanently removed. The decoupled framework provides consistent comparisons across simulations while capturing realistic INP dynamics.

https://doi.org/10.5194/egusphere-2025-3620
Preprint. Discussion started: 6 October 2025

APPENDIX C

Governing equations

Based on the following equations, the simplified 1D aerosol cloud model predicts the budgets for ice-nucleating particles (INPs) and ice particles (Knopf et al., 2023b):

$$\frac{dN_{\mathrm{INP}}^{\mathrm{Imm}}(z_i,t,k_*^{\mathrm{Imm}})}{dt} = -S_{\mathrm{act}}(z_i,t,k_*^{\mathrm{Imm}}) + S_{\mathrm{ent}}(z_i,t,k_*^{\mathrm{Imm}}) + S_{\mathrm{mix}}(z_i,t,k_*^{\mathrm{Imm}}) \quad \text{(C1)}$$

$$\frac{dN_{\mathrm{i}}(z_i,t)}{dt} = \sum\nolimits_{k_*^{\mathrm{Imm}}} S_{\mathrm{act}}\,(z_i,t,k_*^{\mathrm{Imm}}) - S_{\mathrm{i_{sed}}}(z_i,t) + S_{\mathrm{i_{mix}}}(z_i,t)\,, \quad \text{(C2)}$$

where N_{INP} presents the number concentration of activatable INPs and N_{i} denotes the number concentration of ice crystals. The z_i signifies the height at grid cell with index i counted from bottom layer (1, surface) to the top layer (m, PBL top). Notice that the superscript Imm refers to the specific type of IMF parameterization used (INN, INAS, ABIFM or ABIFM*), and k_*^{Imm} represents additional variable dimensions that depend on the chosen IMF parameterizations. For example, for application of INN, k_*^{Imm} is T_{INP} (reflecting the INP temperature arrays), for INAS, k_*^{Imm} is a combination of T_{INP} and d (reflecting a 2D array consisting of INP temperature and diameter arrays), while for ABIFM and ABIFM*, $k_*^{\mathrm{Imm}} = d$. Moreover, the model utilizes several variables to describe the budget terms. S_{act}, S_{ent} and S_{mix} represent the INP activation, cloud-top entrainment, and turbulent mixing budget terms, respectively. For ice particles, $S_{\mathrm{i_{sed}}}$ and $S_{\mathrm{i_{mix}}}$ denote the ice sedimentation and mixing budget terms. It is essential to note that ice crystals do not retain information about their associated INPs. Therefore, the activation budget is summed over the full T_{INP} array (in INN), the T_{INP} and d arrays (in INAS) and the d array (in ABIFM and ABIFM*).

In the model configuration employed in this study, we utilize a time splitting approach to calculate the budgets for ice-nucleating particles (INPs) and ice particles at every time step. The implicit solution for S_{act} is given as

$$S_{\mathrm{act}}\,(z_i,t,k_*^{\mathrm{Imm}}) = \frac{N_{\mathrm{INP}}^{\mathrm{Imm}}(z_i,t,k_*^{\mathrm{Imm}})}{\delta t + \tau_{\mathrm{act}}}\,, \quad \text{(C3)}$$

where the time step length denoted by δt, is set by default to 10 s. For CNT-based parameterizations (ABIFM, ABIFM*), τ_{act} is calculated as $\tau_{\mathrm{act}} = \frac{1}{J_{\mathrm{het}}(T(z_i),a_{\mathrm{w}}(z_i))\pi d^2}$. For deterministic parameterizations (INN, INAS) in this study, INP activation is treated as instantaneous once temperature conditions are met. This is implemented by directly converting the number of activatable INPs (determined by the respective deterministic parameterization at the given temperature) to ice crystals within the model timestep, effectively bypassing the explicit τ_{act}-dependent formulation of S_{act} shown in Eq. (C3) which is used for CNT schemes.The implicit Euler method (Hoffman et al., 2001), is used to ensure numerical stability, where $\delta t \ll \tau_{act}$ relevant for CNT schemes), the change in concentration is proportional to $\frac{-\delta t}{\delta t+\tau_{\mathrm{act}}}$, which becomes increasingly similar to the explicit solution, where the change in concentration is proportional to $\frac{-\delta t}{\tau_{\mathrm{act}}}$. However, this implicit Euler method ensures that the loss never exceeds the initial value.

https://doi.org/10.5194/egusphere-2025-3620
Preprint. Discussion started: 6 October 2025

To ensure numerical stability and avoid violating the Courant-Friedrichs-Lewy (CFL) condition, S_{ent} is computed implicitly:

$$S_{\text{ent}}\left(z_m, t, k_*^{\text{Imm}}\right) = \frac{N_{\text{INP}}^{\text{Imm}}(z_m, t, k_*^{\text{Imm}}) + N_{\text{INP,FT}}^{\text{Imm}}(k_*^{\text{Imm}})}{\left(\delta t + \frac{\delta t}{w_{\text{e}}}\right)}\,, \tag{C4}$$

where w_{e} is the entrainment rate and $N_{\text{INP,FT}}^{\text{Imm}}$ refers to the free-troposphere immersion freezing INP concentration, which is equal to the initial domain INP size distribution. Notice that z_m represents the height of the domain top. Following Fridlind et al. (2012), w_{e} is assumed to be 0.1 cm s^{-1} based on LES results.

The mixing terms for INPs and ice particles are calculated as the following:

$$S_{\text{mix}}(z_i, t, k_*^{\text{Imm}}) = \frac{1}{\tau_{\text{mix}}}(\overline{N_{\text{INP}}^{\text{Imm}}(t, k_*^{\text{Imm}})} - N_{\text{INP}}^{\text{Imm}}(z_i, t, k_*^{\text{Imm}})) \tag{C5}$$

$$S_{\text{i}_{\text{mix}}}(z_i, t) = \frac{1}{\tau_{\text{mix}}}\left(\overline{N_{\text{i}}(t)} - N_{\text{i}}(z_i, t)\right)\,, \tag{C6}$$

where τ_{mix} is the PBL mixing time scale, $\overline{N_{\text{INP}}^{\text{Imm}}}$ is the PBL mean activatable INP number concentration averaged over the whole domain, and $\overline{N_{\text{i}}(t)}$ denotes the PBL mean N_{i}.

Lastly, the sedimentation term for ice crystals is determined as follows:

$$S_{\text{i}_{\text{sed}}}\left(z_i, t\right) = \frac{v_{\text{f}}}{\delta z}\left(N_{\text{i}}(z_{i+1}, t) - N_{\text{i}}(z_i, t)\right)\,, \tag{C7}$$

where v_{f} is the number-weighted ice sedimentation rate (ice crystal fall velocity), maintained as a constant value based on LES estimates of circa 30 cm s^{-1} (Fridlind et al., 2012). To prevent potential numerical instability, we always set the $v_{\text{f}} \cdot \delta t$ to be smaller than δz, thus leading to CFL < 1. Also, note that in Eq. (C7), the i ranges from 1 to m-1 (index of layer below the PBL top) instead of from 1 to m.

As shown above, we account for the loss and gain of INPs and ice crystals, thus, treating the INPs and ice crystals prognostically.

https://doi.org/10.5194/egusphere-2025-3620
Preprint. Discussion started: 6 October 2025

1030

APPENDIX D

Nomenclature

a_w [-]	Water activity
a_w^i [-]	Ice melting point as a function of water activity
d [µm]	INP diameter array
Δa_w [-]	Water activity criterion
δt [s]	Time step length
δz [m]	Model grid cell thickness (vertical resolution)
J_{het} [cm^{-2} s^{-1}]	Heterogeneous ice nucleation rate coefficient
k_*^{Imm} [°C], [°C µm], or [µm]	Additional variable dimensions depending on the applied parameterization
N_{aer} [cm^{-3}]	Aerosol number concentration
$N_{aer>0.5\mu m}$ [cm^{-3}]	Aerosol number concentration for particles larger than 0.5 µm
N_i [L^{-1}]	Ice crystal number concentration
$\overline{N_i(t)}$ [L^{-1}]	PBL mean ice crystal number concentration
N_{INP} [L^{-1}]	Activatable INP number concentration
$\overline{N_{INP}}$ [L^{-1}]	PBL mean activatable INP number concentration
N_{INP}^{Imm} [L^{-1}]	Activatable INP number concentration for given immersion freezing parameterization
$N_{INP,FT}$ [L^{-1}]	Free-troposphere activatable INP concentration
$N_{INP}(T)$ [L^{-1}]	The number concentration of INPs that activate specifically within temperature bin
n_s [cm^{-2}]	Ice nucleation active sites density
RH [%]	Relative humidity expressed in percent
S_{act} [m^{-3} s^{-1}]	INP activation budget term

https://doi.org/10.5194/egusphere-2025-3620
Preprint. Discussion started: 6 October 2025

$S_{\mathrm{act}}^{\mathrm{Imm}}$ [m^{-3}]	INP activation budget term calculated based on the selected immersion freezing parameterizations
$S_{\mathrm{act}}^{\mathrm{sing\ (INN)}}$ [m^{-3}]	INP activation budget term calculated based on the INN
$S_{\mathrm{act}}^{\mathrm{sing\ (INAS)}}$ [m^{-3}]	INP activation budget term calculated based on the INAS
$S_{\mathrm{act}}^{\mathrm{CNT\ (ABIFM)}}$ [m^{-3}]	INP activation budget term calculated based on the ABIFM
S_{ent} [m^{-3} s^{-1}]	Cloud-top entrainment budget term
S_{ice} [-]	Supersaturation with respect to ice
$S_{\mathrm{i_{mix}}}$ [m^{-3} s^{-1}]	Ice mixing budget term
$S_{\mathrm{i_{sed}}}$ [m^{-3} s^{-1}]	Ice sedimentation budget term
S_{mix} [m^{-3} s^{-1}]	Turbulent mixing budget term
t [s]	Model time step
τ_{act} [s]	Activation time scale
T_{INP} [°C]	INP temperature array
τ_{mix} [s]	PBL mixing time scale
v_{f} [m s^{-1}]	ice sedimentation rate
w_{e} [cm s^{-1}]	Entrainment rate
z_i [m]	Height at grid cell index i
z_m [m]	Height at domain top (grid cell index m)
$\mathrm{INP_{array}}$ [m^{-3}]	Three-dimensional array that stores calculated INP values.
$\mathrm{INP_{totarray}}$ [m^{-3}]	The sum of all INPs with activation temperatures warmer than the current cloud conditions that remain available for ice nucleation.

https://doi.org/10.5194/egusphere-2025-3620
Preprint. Discussion started: 6 October 2025

APPENDIX E

List of Abbreviations

2D-C	Two-dimensional cloud optical array probes
2D-P	Two-dimensional precipitation optical array probes
ABIFM	The water-activity-based immersion freezing model
ABIFM*	The water-activity-based immersion freezing model which enables immersion freezing commencing under subsaturated conditions
CCR	Cloud cooling rate
CFL	Courant–Friedrichs–Lewy condition
CNT	Classical nucleation theory
CPI	Cloud Particle Imager
DHARMA	Distributed Hydrodynamic Aerosol and Radiative Modeling Application
ICEALOT	International Chemistry Experiment in the Arctic Lower Troposphere
INAS	Ice nucleation active sites-based parameterization
INN	Ice nucleation number-based parameterization
INP	Ice nucleating particle
ISDAC	Indirect and Semi-Direct Aerosol Campaign
LES	Large-eddy simulation
MMCR	Millimeter Wavelength Cloud Radar
M-PACE	Mixed-Phase Arctic Cloud Experiment
MPC	Mixed-phase cloud
PBL	Planetary boundary layer
PSD	Particle size distribution
SHEBA	The Surface Heat Budget of the Arctic campaign
SSA	Sea spray aerosol

https://doi.org/10.5194/egusphere-2025-3620
Preprint. Discussion started: 6 October 2025

Code and data availability. The 1D model version used in this manuscript is available on Zenodo at https://doi.org/10.5281/zenodo.7108690 (Silber et al., 2022). The most current version of the model is available on Zenodo at https://doi.org/10.5281/zenodo.16414825 (Sun et al., 2025a). The model output data is available on Zenodo at https://doi.org/10.5281/zenodo.16413525 (Sun et al., 2025b). The data analysis and plotting scripts for the manuscript is available on Zenodo at https://doi.org/10.5281/zenodo.16414282 (Sun et al., 2025c).

Author contributions. YS modified the Python code of the 1D-AC model with guidance from IS, performed all sensitivity tests, and wrote the first draft of the paper, DAK supervised the project. DAK, IS, NR, and AMF assisted in methodology and results validation. All authors discussed interpretation of the data and contributed to writing and reviewing of the paper.

Competing interests. The contact author has declared that none of the authors has any competing interests.

Disclaimer. Publisher's note: Copernicus Publications remains neutral with regard to jurisdictional claims in published maps and institutional affiliations.

Acknowledgements. This study was supported by the U.S. Department of Energy's Atmospheric System Research, an Office of Science Biological and Environmental Research program, under Grant DE-SC0021034.

Financial support. This study was supported by the U.S. Department of Energy's Atmospheric System Research, an Office of Science Biological and Environmental Research program, Grant DE-SC0021034.

https://doi.org/10.5194/egusphere-2025-3620
Preprint. Discussion started: 6 October 2025

References

Ackerman, A. S., Toon, O. B., Stevens, D. E., Heymsfield, A. J., Ramanathan, V. V., and Welton, E. J.: Reduction of tropical cloudiness by soot, Science, 288, 1042-1047, https://doi.org/10.1126/science.288.5468.1042, 2000.

Alpert, P. A., 2022.

Alpert, P. A. and Knopf, D. A.: Analysis of isothermal and cooling-rate-dependent immersion freezing by a unifying stochastic ice nucleation model, Atmos. Chem. Phys., 16, 2083-2107, https://doi.org/10.5194/acp-16-2083-2016, 2016.

Alpert, P. A., Kilthau, W. P., O'Brien, R. E., Moffet, R. C., Gilles, M. K., Wang, B., Laskin, A., Aller, J. Y., and Knopf, D. A.: Ice-nucleating agents in sea spray aerosol identified and quantified with a holistic multimodal freezing model, Sci. Adv., 8, eabq6842, https://doi.org/10.1126/sciadv.abq6842, 2022.

Andronache, C.: Characterization of Mixed-Phase Clouds: Contributions From the Field Campaigns and Ground Based Networks, in: Mixed-Phase Clouds, edited by: Andronache, C., Elsevier, 97-120, https://doi.org/10.1016/b978-0-12-810549-8.00005-2, 2018.

Ansmann, A., Tesche, M., Althausen, D., Müller, D., Seifert, P., Freudenthaler, V., Heese, B., Wiegner, M., Pisani, G., Knippertz, P., and Dubovik, O.: Influence of Saharan dust on cloud glaciation in southern Morocco during the Saharan Mineral Dust Experiment, J. Geophys. Res.-Atmos., 113, https://doi.org/10.1029/2007jd008785, 2008.

Arabas, S., Curtis, J. H., Silber, I., Fridlind, A. M., Knopf, D. A., West, M., and Riemer, N.: Immersion Freezing in Particle-Based Aerosol-Cloud Microphysics: A Probabilistic Perspective on Singular and Time-Dependent Models, J Adv Model Earth Sy, 17, e2024MS004770, https://doi.org/https://doi.org/10.1029/2024MS004770, 2025.

Avramov, A., Ackerman, A. S., Fridlind, A. M., van Diedenhoven, B., Botta, G., Aydin, K., Verlinde, J., Korolev, A. V., Strapp, J. W., McFarquhar, G. M., Jackson, R., Brooks, S. D., Glen, A., and Wolde, M.: Toward ice formation closure in Arctic mixed-phase boundary layer clouds during ISDAC, J. Geophys. Res.-Atmos., 116, https://doi.org/10.1029/2011jd015910, 2011.

Bauer, S. E., Wright, D. L., Koch, D., Lewis, E. R., McGraw, R., Chang, L. S., Schwartz, S. E., and Ruedy, R.: MATRIX (Multiconfiguration Aerosol TRacker of mIXing state): an aerosol microphysical module for global atmospheric models, Atmos. Chem. Phys., 8, 6003-6035, https://doi.org/10.5194/acp-8-6003-2008, 2008.

Bergman, T., Makkonen, R., Schrödner, R., Swietlicki, E., Phillips, V. T. J., Le Sager, P., and van Noije, T.: Description and evaluation of a secondary organic aerosol and new particle formation scheme within TM5-MP v1.2, Geosci. Model Dev., 15, 683-713, https://doi.org/10.5194/gmd-15-683-2022, 2022.

Biermann, U. M., Presper, T., Koop, T., Mossinger, J., Crutzen, P. J., and Peter, T.: The unsuitability of meteoritic and other nuclei for polar stratospheric cloud freezing, Geophys. Res. Lett., 23, 1693-1696, https://doi.org/10.1029/96gl01577, 1996.

Bigg, E. K.: The Supercooling of Water, Proc. Phys. Soc., 66, 688-694, https://doi.org/10.1088/0370-1301/66/8/309, 1953.

Boose, Y., Sierau, B., García, M. I., Rodríguez, S., Alastuey, A., Linke, C., Schnaiter, M., Kupiszewski, P., Kanji, Z. A., and Lohmann, U.: Ice nucleating particles in the Saharan Air Layer, Atmos. Chem. Phys., 16, 9067-9087, https://doi.org/10.5194/acp-16-9067-2016, 2016.

Burrows, S. M., Hoose, C., Pöschl, U., and Lawrence, M. G.: Ice nuclei in marine air: biogenic particles or dust?, Atmos. Chem. Phys., 13, 245-267, https://doi.org/10.5194/acp-13-245-2013, 2013.

Burrows, S. M., McCluskey, C. S., Cornwell, G., Steinke, I., Zhang, K., Zhao, B., Zawadowicz, M., Raman, A., Kulkarni, G., China, S., Zelenyuk, A., and DeMott, P. J.: Ice-Nucleating Particles That Impact Clouds and Climate: Observational and Modeling Research Needs, Rev Geophys, 60, e2021RG000745, https://doi.org/10.1029/2021RG000745, 2022.

China, S., Alpert, P. A., Zhang, B., Schum, S., Dzepina, K., Wright, K., Owen, R. C., Fialho, P., Mazzoleni, L. R., Mazzoleni, C., and Knopf, D. A.: Ice cloud formation potential by free tropospheric particles from long-range transport over the Northern Atlantic Ocean, J. Geophys. Res.-Atmos., 122, 3065-3079, https://doi.org/10.1002/2016jd025817, 2017.

Chou, C., Stetzer, O., Weingartner, E., Jurányi, Z., Kanji, Z. A., and Lohmann, U.: Ice nuclei properties within a Saharan dust event at the Jungfraujoch in the Swiss Alps, Atmos. Chem. Phys., 11, 4725-4738, https://doi.org/10.5194/acp-11-4725-2011, 2011.

Curry, J. A., Hobbs, P. V., King, M. D., Randall, D. A., and Minnis, P.: FIRE arctic clouds experiment, Bull. Am. Meteorol. Soc., 81, 5-30, https://doi.org/10.1175/1520-0477(2000)081<0005:FACE>2.3.CO;2, 2000.

de Boer, G., Morrison, H., Shupe, M. D., and Hildner, R.: Evidence of liquid dependent ice nucleation in high-latitude stratiform clouds from surface remote sensors, Geophys. Res. Lett., 38, L01803, https://doi.org/10.1029/2010gl046016, 2011.

Deck, L. T., Ochsenbein, D. R., and Mazzotti, M.: Stochastic ice nucleation governs the freezing process of biopharmaceuticals in vials, Int. J. Pharm., 625, 122051, https://doi.org/10.1016/j.ijpharm.2022.122051, 2022.

DeMott, P. J., Cziczo, D. J., Prenni, A. J., Murphy, D. M., Kreidenweis, S. M., Thomson, D. S., Borys, R., and Rogers, D. C.: Measurements of the concentration and composition of nuclei for cirrus formation, Proc. Nat. Acad. Sci., 100, 14655-14660, https://doi.org/10.1073/pnas.2532677100, 2003.

DeMott, P. J., Prenni, A. J., Liu, X., Kreidenweis, S. M., Petters, M. D., Twohy, C. H., Richardson, M. S., Eidhammer, T., and Rogers, D. C.: Predicting global atmospheric ice nuclei distributions and their impacts on climate, Proc. Nat. Acad. Sci., 107, 11217-11222, https://doi.org/10.1073/pnas.0910818107, 2010.

https://doi.org/10.5194/egusphere-2025-3620
Preprint. Discussion started: 6 October 2025

DeMott, P. J., Prenni, A. J., McMeeking, G. R., Sullivan, R. C., Petters, M. D., Tobo, Y., Niemand, M., Möhler, O., Snider, J. R., Wang, Z., and Kreidenweis, S. M.: Integrating laboratory and field data to quantify the immersion freezing ice nucleation activity of mineral dust particles, Atmos. Chem. Phys., 15, 393-409, https://doi.org/10.5194/acp-15-393-2015, 2015.

Dong, X. Q. and Mace, G. G.: Arctic stratus cloud properties and radiative forcing derived from ground-based data collected at Barrow, Alaska, J. Climate, 16, 445-461, https://doi.org/10.1175/1520-0442(2003)016<0445:Ascpar>2.0.Co;2, 2003.

Earle, M. E., Liu, P. S. K., Strapp, J. W., Zelenyuk, A., Imre, D., McFarquhar, G. M., Shantz, N. C., and Leaitch, W. R.: Factors influencing the microphysics and radiative properties of liquid-dominated Arctic clouds: Insight from observations of aerosol and clouds during ISDAC, J. Geophys. Res.-Atmos., 116, 16, https://doi.org/Artn D00t09 10.1029/2011jd015887, 2011.

Fan, J. W., Ovtchinnikov, M., Comstock, J. M., McFarlane, S. A., and Khain, A.: Ice formation in Arctic mixed-phase clouds: Insights from a 3-D cloud-resolving model with size-resolved aerosol and cloud microphysics, J. Geophys. Res.-Atmos., 114, https://doi.org/10.1029/2008jd010782, 2009.

Field, P. R. and Heymsfield, A. J.: Importance of snow to global precipitation, Geophys. Res. Lett., 42, 9512-9520, https://doi.org/10.1002/2015gl065497, 2015.

Fridlind, A. M. and Ackerman, A. S.: Simulations of Arctic Mixed-Phase Boundary Layer Clouds: Advances in Understanding and Outstanding Questions, in: Mixed-Phase Clouds, edited by: Andronache, C., Elsevier, 153-183, https://doi.org/10.1016/b978-0-12-810549-8.00007-6, 2018.

Fridlind, A. M., Ackerman, A. S., McFarquhar, G., Zhang, G., Poellot, M. R., DeMott, P. J., Prenni, A. J., and Heymsfield, A. J.: Ice properties of single-layer stratocumulus during the Mixed-Phase Arctic Cloud Experiment: 2. Model results, J. Geophys. Res.-Atmos., 112, https://doi.org/10.1029/2007jd008646, 2007.

Fridlind, A. M., van Diedenhoven, B., Ackerman, A. S., Avramov, A., Mrowiec, A., Morrison, H., Zuidema, P., and Shupe, M. D.: A FIRE-ACE/SHEBA Case Study of Mixed-Phase Arctic Boundary Layer Clouds: Entrainment Rate Limitations on Rapid Primary Ice Nucleation Processes, J. Atmos. Sci., 69, 365-389, https://doi.org/10.1175/Jas-D-11-052.1, 2012.

Friedman, B., Kulkarni, G., Beránek, J., Zelenyuk, A., Thornton, J. A., and Cziczo, D. J.: Ice nucleation and droplet formation by bare and coated soot particles, J. Geophys. Res.-Atmos., 116, https://doi.org/10.1029/2011JD015999, 2011.

Gulev, S. K., P.W. Thorne, J. Ahn, F.J. Dentener, C.M. Domingues, S. Gerland, D. Gong, D.S. Kaufman, H.C. Nnamchi, J. Quaas, J.A. Rivera, S. Sathyendranath, S.L. Smith, B. Trewin, K. von Schuckmann, and R.S. Vose: Changing State of the Climate System. In Climate Change 2021: The Physical Science Basis. Contribution of Working Group I to the Sixth Assessment Report of the Intergovernmental Panel on Climate Change, in, edited by: Masson-Delmotte, V., P. Z., A. Pirani, S.L. Connors, C. Péan, S. Berger, N. Caud, Y. Chen, L. Goldfarb, M.I. Gomis, M. Huang, K. Leitzell, E. Lonnoy, J.B.R. Matthews, T.K. Maycock, T. Waterfield, O. Yelekçi, R. Yu, and B. Zhou, Cambridge University Press, Cambridge, United Kingdom and New York, NY, USA, 287-422, https://doi.org/10.1017/9781009157896.004., 2021.

Hahn, L. C., Armour, K. C., Zelinka, M. D., Bitz, C. M., and Donohoe, A.: Contributions to Polar Amplification in CMIP5 and CMIP6 Models, Front. Earth Sci., 9, https://doi.org/10.3389/feart.2021.710036, 2021.

Hallett, J. and Mossop, S. C.: Production of secondary ice particles during the riming process, Nature, 249, 26-28, https://doi.org/10.1038/249026a0, 1974.

Hallquist, M., Wenger, J. C., Baltensperger, U., Rudich, Y., Simpson, D., Claeys, M., Dommen, J., Donahue, N. M., George, C., Goldstein, A. H., Hamilton, J. F., Herrmann, H., Hoffmann, T., Iinuma, Y., Jang, M., Jenkin, M. E., Jimenez, J. L., Kiendler-Scharr, A., Maenhaut, W., McFiggans, G., Mentel, T. F., Monod, A., Prévôt, A. S. H., Seinfeld, J. H., Surratt, J. D., Szmigielski, R., and Wildt, J.: The formation, properties and impact of secondary organic aerosol: current and emerging issues, Atmos. Chem. Phys., 9, 5155-5236, https://doi.org/10.5194/acp-9-5155-2009, 2009.

Harrington, J. Y. and Olsson, P. Q.: On the potential influence of ice nuclei on surface-forced marine stratocumulus cloud dynamics, J. Geophys. Res.-Atmos., 106, 27473-27484, https://doi.org/10.1029/2000jd000236, 2001.

Hiranuma, N., Paukert, M., Steinke, I., Zhang, K., Kulkarni, G., Hoose, C., Schnaiter, M., Saathoff, H., and Möhler, O.: A comprehensive parameterization of heterogeneous ice nucleation of dust surrogate: laboratory study with hematite particles and its application to atmospheric models, Atmos. Chem. Phys., 14, 13145-13158, https://doi.org/10.5194/acp-14-13145-2014, 2014.

Hiranuma, N., Brooks, S. D., Moffet, R. C., Glen, A., Laskin, A., Gilles, M. K., Liu, P., Macdonald, A. M., Strapp, J. W., and McFarquhar, G. M.: Chemical characterization of individual particles and residuals of cloud droplets and ice crystals collected on board research aircraft in the ISDAC 2008 study, J. Geophys. Res.-Atmos., 118, 6564-6579, https://doi.org/10.1002/jgrd.50484, 2013.

Hoffman, J. D. and Frankel, S.: Numerical Methods for Engineers and Scientists, Second Edition, Taylor & Francis2001.

Holland, M. M. and Bitz, C. M.: Polar amplification of climate change in coupled models, Climate Dynam., 21, 221-232, https://doi.org/10.1007/s00382-003-0332-6, 2003.

Hoose, C. and Mohler, O.: Heterogeneous ice nucleation on atmospheric aerosols: a review of results from laboratory experiments, Atmos Chem Phys, 12, 9817-9854, https://doi.org/10.5194/acp-12-9817-2012, 2012a.

Hoose, C. and Möhler, O.: Heterogeneous ice nucleation on atmospheric aerosols: a review of results from laboratory experiments, Atmos. Chem. Phys., 12, 9817-9854, https://doi.org/10.5194/acp-12-9817-2012, 2012b.

https://doi.org/10.5194/egusphere-2025-3620
Preprint. Discussion started: 6 October 2025

Hoose, C., Kristjánsson, J. E., Chen, J. P., and Hazra, A.: A Classical-Theory-Based Parameterization of Heterogeneous Ice Nucleation by Mineral Dust, Soot, and Biological Particles in a Global Climate Model, J. Atmos. Sci., 67, 2483-2503, https://doi.org/10.1175/2010jas3425.1, 2010.

Huang, W. T. K., Ickes, L., Tegen, I., Rinaldi, M., Ceburnis, D., and Lohmann, U.: Global relevance of marine organic aerosol as ice nucleating particles, Atmos. Chem. Phys., 18, 11423-11445, https://doi.org/10.5194/acp-18-11423-2018, 2018.

Kanji, Z. A., Welti, A., Corbin, J. C., and Mensah, A. A.: Black Carbon Particles Do Not Matter for Immersion Mode Ice Nucleation, Geophys. Res. Lett., 47, e2019GL086764, https://doi.org/10.1029/2019GL086764, 2020.

Kanji, Z. A., Ladino, L. A., Wex, H., Boose, Y., Burkert-Kohn, M., Cziczo, D. J., and Krämer, M.: Overview of Ice Nucleating Particles, Meteor Mon, 58, 1.1-1.33, https://doi.org/10.1175/Amsmonographs-D-16-0006.1, 2017.

Kawai, K., Matsui, H., and Tobo, Y.: Dominant Role of Arctic Dust With High Ice Nucleating Ability in the Arctic Lower Troposphere, Geophys. Res. Lett., 50, e2022GL102470, https://doi.org/10.1029/2022GL102470, 2023.

Keinert, A., Spannagel, D., Leisner, T., and Kiselev, A.: Secondary Ice Production upon Freezing of Freely Falling Drizzle Droplets, J. Atmos. Sci., 77, 2959-2967, https://doi.org/10.1175/Jas-D-20-0081.1, 2020.

Khain, A., Pinsky, M., and Korolev, A.: Combined Effect of the Wegener–Bergeron–Findeisen Mechanism and Large Eddies on Microphysics of Mixed-Phase Stratiform Clouds, Journal of the Atmospheric Sciences, 79, 383-407, https://doi.org/https://doi.org/10.1175/JAS-D-20-0269.1, 2022.

Knopf, D. A. and Alpert, P. A.: A water activity based model of heterogeneous ice nucleation kinetics for freezing of water and aqueous solution droplets, Faraday Discuss., 165, 513-534, https://doi.org/10.1039/c3fd00035d, 2013.

Knopf, D. A. and Alpert, P. A.: Atmospheric ice nucleation, Nat. Rev. Phys., 5, 203-217, https://doi.org/10.1038/s42254-023-00570-7, 2023a.

Knopf, D. A., Alpert, P. A., and Wang, B. B.: The Role of Organic Aerosol in Atmospheric Ice Nucleation: A Review, Acs Earth Space Chem, 2, 168-202, https://doi.org/10.1021/acsearthspacechem.7b00120, 2018.

Knopf, D. A., Alpert, P. A., Zipori, A., Reicher, N., and Rudich, Y.: Stochastic nucleation processes and substrate abundance explain time-dependent freezing in supercooled droplets, npj clim. atmos. sci., 3, 2, https://doi.org/10.1038/s41612-020-0106-4, 2020.

Knopf, D. A., Silber, I., Riemer, N., Fridlind, A. M., and Ackerman, A. S.: A 1D Model for Nucleation of Ice From Aerosol Particles: An Application to a Mixed-Phase Arctic Stratus Cloud Layer, J. Adv. Model. Earth Sys., 15, e2023MS003663, https://doi.org/10.1029/2023MS003663, 2023b.

Knopf, D. A., Wang, B., Laskin, A., Moffet, R. C., and Gilles, M. K.: Heterogeneous nucleation of ice on anthropogenic organic particles collected in Mexico City, Geophys. Res. Lett., 37, https://doi.org/10.1029/2010gl043362, 2010.

Knopf, D. A., Alpert, P. A., Wang, B., O'Brien, R. E., Kelly, S. T., Laskin, A., Gilles, M. K., and Moffet, R. C.: Microspectroscopic imaging and characterization of individually identified ice nucleating particles from a case field study, J. Geophys. Res.-Atmos., 119, 10,365-310,381, https://doi.org/10.1002/2014jd021866, 2014.

Knopf, D. A., Barry, K. R., Brubaker, T. A., Jahl, L. G., Jankowski, K. A., Li, J., Lu, Y., Monroe, L. W., Moore, K. A., Rivera-Adorno, F. A., Sauceda, K. A., Shi, Y., Tomlin, J. M., Vepuri, H. S. K., Wang, P., Lata, N. N., Levin, E. J. T., Creamean, J. M., Hill, T. C. J., China, S., Alpert, P. A., Moffet, R. C., Hiranuma, N., Sullivan, R. C., Fridlind, A. M., West, M., Riemer, N., Laskin, A., DeMott, P. J., and Liu, X.: Aerosol-Ice Formation Closure: A Southern Great Plains Field Campaign, Bull. Am. Meteorol. Soc., 102, E1952-E1971, https://doi.org/10.1175/Bams-D-20-0151.1, 2021.

Koop, T. and Zobrist, B.: Parameterizations for ice nucleation in biological and atmospheric systems, Phys. Chem. Chem. Phys., 11, 10839-10850, https://doi.org/10.1039/b914289d, 2009.

Koop, T., Luo, B., Tsias, A., and Peter, T.: Water activity as the determinant for homogeneous ice nucleation in aqueous solutions, Nature, 406, 611-614, https://doi.org/10.1038/35020537, 2000.

Koop, T., Luo, B. P., Biermann, U. M., Crutzen, P. J., and Peter, T.: Freezing of HNO3/H2SO4/H2O solutions at stratospheric temperatures: Nucleation statistics and experiments, J. Phys. Chem., 101, 1117-1133, https://doi.org/10.1021/jp9626531, 1997.

Korolev, A. and Leisner, T.: Review of experimental studies of secondary ice production, Atmos. Chem. Phys., 20, 11767-11797, https://doi.org/10.5194/acp-20-11767-2020, 2020a.

Korolev, A., Heckman, I., Wolde, M., Ackerman, A. S., Fridlind, A. M., Ladino, L. A., Lawson, R. P., Milbrandt, J., and Williams, E.: A new look at the environmental conditions favorable to secondary ice production, Atmos. Chem. Phys., 20, 1391-1429, https://doi.org/10.5194/acp-20-1391-2020, 2020b.

Korolev, A., McFarquhar, G., Field, P. R., Franklin, C., Lawson, P., Wang, Z., Williams, E., Abel, S. J., Axisa, D., Borrmann, S., Crosier, J., Fugal, J., Kramer, M., Lohmann, U., Schlenczek, O., Schnaiter, M., and Wendisch, M.: Mixed-Phase Clouds: Progress and Challenges, Meteor Mon, 58, 5.1-5.50, https://doi.org/10.1175/Amsmonographs-D-17-0001.1, 2017.

Korolev, A. V., Isaac, G. A., Cober, S. G., Strapp, J. W., and Hallett, J.: Microphysical characterization of mixed-phase clouds, Quart. J. Roy. Meteor. Soc., 129, 39-65, https://doi.org/10.1256/qj.01.204, 2003.

Lauber, A., Kiselev, A., Pander, T., Handmann, P., and Leisner, T.: Secondary Ice Formation during Freezing of Levitated Droplet, J. Atmos. Sci., 75, 2815-2826, https://doi.org/10.1175/Jas-D-18-0052.1, 2018.

https://doi.org/10.5194/egusphere-2025-3620
Preprint. Discussion started: 6 October 2025

Levine, J.: Statistical explanation of spontaneous freezing of water droplets, National Advisory Committee for AeronauticsNACA-TN-2234,1950.
Liu, X., Ma, P. L., Wang, H., Tilmes, S., Singh, B., Easter, R. C., Ghan, S. J., and Rasch, P. J.: Description and evaluation of a new four-mode version of the Modal Aerosol Module (MAM4) within version 5.3 of the Community Atmosphere Model, Geosci. Model Dev., 9, 505-522, https://doi.org/10.5194/gmd-9-505-2016, 2016.
Lubin, D., Zhang, D., Silber, I., Scott, R. C., Kalogeras, P., Battaglia, A., Bromwich, D. H., Cadeddu, M., Eloranta, E., Fridlind, A., Frossard, A., Hines, K. M., Kneifel, S., Leaitch, W. R., Lin, W., Nicolas, J., Powers, H., Quinn, P. K., Rowe, P., Russell, L. M., Sharma, S., Verlinde, J., and Vogelmann, A. M.: AWARE: The Atmospheric Radiation Measurement (ARM) West Antarctic Radiation Experiment, Bull. Am. Meteorol. Soc., 101, E1069-E1091, https://doi.org/10.1175/BAMS-D-18-0278.1, 2020.
Luke, E. P., Yang, F., Kollias, P., Vogelmann, A. M., and Maahn, M.: New insights into ice multiplication using remote-sensing observations of slightly supercooled mixed-phase clouds in the Arctic, Proc. Nat. Acad. Sci., 118, e2021387118, https://doi.org/10.1073/pnas.2021387118, 2021.
McCluskey, C. S., DeMott, P. J., Ma, P. L., and Burrows, S. M.: Numerical Representations of Marine Ice-Nucleating Particles in Remote Marine Environments Evaluated Against Observations, Geophys. Res. Lett., 46, 7838-7847, https://doi.org/10.1029/2018gl081861, 2019.
McCluskey, C. S., Ovadnevaite, J., Rinaldi, M., Atkinson, J., Belosi, F., Ceburnis, D., Marullo, S., Hill, T. C. J., Lohmann, U., Kanji, Z. A., O'Dowd, C., Kreidenweis, S. M., and DeMott, P. J.: Marine and Terrestrial Organic Ice-Nucleating Particles in Pristine Marine to Continentally Influenced Northeast Atlantic Air Masses, J. Geophys. Res.-Atmos., 123, 6196-6212, https://doi.org/10.1029/2017jd028033, 2018.
McFarquhar, G. M., Ghan, S., Verlinde, J., Korolev, A., Strapp, J. W., Schmid, B., Tomlinson, J. M., Wolde, M., Brooks, S. D., Cziczo, D., Dubey, M. K., Fan, J. W., Flynn, C., Gultepe, I., Hubbe, J., Gilles, M. K., Laskin, A., Lawson, P., Leaitch, W. R., Liu, P., Liu, X. H., Lubin, D., Mazzoleni, C., Macdonald, A. M., Moffet, R. C., Morrison, H., Ovchinnikov, M., Shupe, M. D., Turner, D. D., Xie, S. C., Zelenyuk, A., Bae, K., Freer, M., and Glen, A.: INDIRECT AND SEMI-DIRECT AEROSOL CAMPAIGN The Impact of Arctic Aerosols on Clouds, Bull. Am. Meteorol. Soc., 92, 183-201, https://doi.org/10.1175/2010bams2935.1, 2011.
Miltenberger, A. K. and Field, P. R.: Sensitivity of mixed-phase moderately deep convective clouds to parameterizations of ice formation - an ensemble perspective, Atmos. Chem. Phys., 21, 3627-3642, https://doi.org/10.5194/acp-21-3627-2021, 2021.
Morice, C. P., Kennedy, J. J., Rayner, N. A., Winn, J. P., Hogan, E., Killick, R. E., Dunn, R. J. H., Osborn, T. J., Jones, P. D., and Simpson, I. R.: An Updated Assessment of Near-Surface Temperature Change From 1850: The HadCRUT5 Data Set, J. Geophys. Res.-Atmos., 126, e2019JD032361, https://doi.org/10.1029/2019JD032361, 2021.
Morrison, H.: On the robustness of aerosol effects on an idealized supercell storm simulated with a cloud system-resolving model, Atmos. Chem. Phys., 12, 7689-7705, https://doi.org/10.5194/acp-12-7689-2012, 2012.
Morrison, H., Curry, J. A., and Khvorostyanov, V. I.: A new double-moment microphysics parameterization for application in cloud and climate models. Part I: Description, J. Atmos. Sci., 62, 1665-1677, https://doi.org/10.1175/Jas3446.1, 2005.
Morrison, H., Zuidema, P., Ackerman, A. S., Avramov, A., de Boer, G., Fan, J. W., Fridlind, A. M., Hashino, T., Harrington, J. Y., Luo, Y. L., Ovchinnikov, M., and Shipway, B.: Intercomparison of cloud model simulations of Arctic mixed-phase boundary layer clouds observed during SHEBA/FIRE-ACE, J. Adv. Model. Earth Sys., 3, https://doi.org/10.1029/2011ms000066, 2011.
Morrison, H., van Lier-Walqui, M., Fridlind, A. M., Grabowski, W. W., Harrington, J. Y., Hoose, C., Korolev, A., Kumjian, M. R., Milbrandt, J. A., Pawlowska, H., Posselt, D. J., Prat, O. P., Reimel, K. J., Shima, S.-I., van Diedenhoven, B., and Xue, L.: Confronting the Challenge of Modeling Cloud and Precipitation Microphysics, J. Adv. Model. Earth Sys., 12, e2019MS001689, https://doi.org/10.1029/2019MS001689, 2020.
Mülmenstädt, J., Sourdeval, O., Delanoë, J., and Quaas, J.: Frequency of occurrence of rain from liquid-, mixed-, and ice-phase clouds derived from A-Train satellite retrievals, Geophys. Res. Lett., 42, 6502-6509, https://doi.org/10.1002/2015gl064604, 2015.
Murray, B. J., O'Sullivan, D., Atkinson, J. D., and Webb, M. E.: Ice nucleation by particles immersed in supercooled cloud droplets, Chem. Soc. Rev., 41, 6519-6554, https://doi.org/10.1039/c2cs35200a, 2012.
Niemand, M., Möhler, O., Vogel, B., Vogel, H., Hoose, C., Connolly, P., Klein, H., Bingemer, H., DeMott, P., Skrotzki, J., and Leisner, T.: A Particle-Surface-Area-Based Parameterization of Immersion Freezing on Desert Dust Particles, J. Atmos. Sci., 69, 3077-3092, https://doi.org/10.1175/Jas-D-11-0249.1, 2012.
Ovchinnikov, M., Ackerman, A. S., Avramov, A., Cheng, A., Fan, J., Fridlind, A. M., Ghan, S., Harrington, J., Hoose, C., Korolev, A., McFarquhar, G. M., Morrison, H., Paukert, M., Savre, J., Shipway, B. J., Shupe, M. D., Solomon, A., and Sulia, K.: Intercomparison of large-eddy simulations of Arctic mixed-phase clouds: Importance of ice size distribution assumptions, J Adv Model Earth Sy, 6, 223-248, https://doi.org/https://doi.org/10.1002/2013MS000282, 2014.
Penner, J. E., Zhou, C., Garnier, A., and Mitchell, D. L.: Anthropogenic Aerosol Indirect Effects in Cirrus Clouds, J. Geophys. Res.-Atmos., 123, 11652-11677, https://doi.org/10.1029/2018JD029204, 2018.
Phillips, V. T. J., Patade, S., Gutierrez, J., and Bansemer, A.: Secondary Ice Production by Fragmentation of Freezing Drops: Formulation and Theory, J. Atmos. Sci., 75, 3031-3070, https://doi.org/10.1175/Jas-D-17-0190.1, 2018.

https://doi.org/10.5194/egusphere-2025-3620
Preprint. Discussion started: 6 October 2025

Phillips, V. T. J., Yano, J. I., Formenton, M., Ilotoviz, E., Kanawade, V., Kudzotsa, I., Sun, J. M., Bansemer, A., Detwiler, A. G., Khain, A., and Tessendorf, S. A.: Ice Multiplication by Breakup in Ice-Ice Collisions. Part II: Numerical Simulations, J. Atmos. Sci., 74, 2789-2811, https://doi.org/10.1175/Jas-D-16-0223.1, 2017.
Prenni, A. J., Petters, M. D., Kreidenweis, S. M., Heald, C. L., Martin, S. T., Artaxo, P., Garland, R. M., Wollny, A. G., and Pöschl, U.: Relative roles of biogenic emissions and Saharan dust as ice nuclei in the Amazon basin, Nature Geosci., 2, 401-404, https://doi.org/10.1038/Ngeo517, 2009.
Pruppacher, H. R. and Klett, J. D.: Heterogeneous Nucleation, in: Microphysics of Clouds and Precipitation, edited by: Pruppacher, H. R., and Klett, J. D., Atmospheric and Oceanographic Sciences Library, Springer Netherlands, Dordrecht, 287-360, https://doi.org/10.1007/978-0-306-48100-0_9, 2010.
Quinn, P. K., Coffman, D. J., Johnson, J. E., Upchurch, L. M., and Bates, T. S.: Small fraction of marine cloud condensation nuclei made up of sea spray aerosol, Nature Geosci., 10, 674-+, https://doi.org/10.1038/Ngeo3003, 2017.
Raatikainen, T., Prank, M., Ahola, J., Kokkola, H., Tonttila, J., and Romakkaniemi, S.: The effect of marine ice-nucleating particles on mixed-phase clouds, Atmos. Chem. Phys., 22, 3763-3778, https://doi.org/10.5194/acp-22-3763-2022, 2022.
Richter-Menge, J., Jeffries, M. O., and Osborne, E: The Arctic in "State of the Climate in 2017", Bull. Am. Meteorol. Soc., 99, 143–173, https://doi.org/10.1175/2018BAMSStateoftheClimate.1, 2018.
Riemer, N., Ault, A. P., West, M., Craig, R. L., and Curtis, J. H.: Aerosol Mixing State: Measurements, Modeling, and Impacts, Rev Geophys, 57, 187-249, https://doi.org/10.1029/2018RG000615, 2019.
Savre, J. and Ekman, A. M. L.: Large-eddy simulation of three mixed-phase cloud events during ISDAC: Conditions for persistent heterogeneous ice formation, J. Geophys. Res.-Atmos., 120, 7699-7725, https://doi.org/10.1002/2014jd023006, 2015.
Schill, G. P., DeMott, P. J., Levin, E. J. T., and Kreidenweis, S. M.: Use of the Single Particle Soot Photometer (SP2) as a pre-filter for ice nucleation measurements: effect of particle mixing state and determination of SP2 conditions to fully vaporize refractory black carbon, Atmos. Meas. Tech., 11, 3007-3020, https://doi.org/10.5194/amt-11-3007-2018, 2018.
Schill, G. P., DeMott, P. J., Emerson, E. W., Rauker, A. M. C., Kodros, J. K., Suski, K. J., Hill, T. C. J., Levin, E. J. T., Pierce, J. R., Farmer, D. K., and Kreidenweis, S. M.: The contribution of black carbon to global ice nucleating particle concentrations relevant to mixed-phase clouds, Proc. Nat. Acad. Sci., 117, 22705-22711, https://doi.org/doi:10.1073/pnas.2001674117, 2020.
Schmale, J., Zieger, P., and Ekman, A. M. L.: Aerosols in current and future Arctic climate, Nat. Clim. Change, 11, 95-105, https://doi.org/10.1038/s41558-020-00969-5, 2021.
Serreze, M. C. and Barry, R. G.: Processes and impacts of Arctic amplification: A research synthesis, Glob. Planet. Change, 77, 85-96, https://doi.org/10.1016/j.gloplacha.2011.03.004, 2011.
Shi, Y., Liu, X. H., Wu, M. X., Zhao, X., Ke, Z. M., and Brown, H.: Relative importance of high-latitude local and long-range-transported dust for Arctic ice-nucleating particles and impacts on Arctic mixed-phase clouds, Atmos. Chem. Phys., 22, 2909-2935, https://doi.org/10.5194/acp-22-2909-2022, 2022.
Shrivastava, M., Cappa, C. D., Fan, J. W., Goldstein, A. H., Guenther, A. B., Jimenez, J. L., Kuang, C., Laskin, A., Martin, S. T., Ng, N. L., Petaja, T., Pierce, J. R., Rasch, P. J., Roldin, P., Seinfeld, J. H., Shilling, J., Smith, J. N., Thornton, J. A., Volkamer, R., Wang, J., Worsnop, D. R., Zaveri, R. A., Zelenyuk, A., and Zhang, Q.: Recent advances in understanding secondary organic aerosol: Implications for global climate forcing, Rev Geophys, 55, 509-559, https://doi.org/10.1002/2016rg000540, 2017.
Shupe, M. D.: Clouds at Arctic Atmospheric Observatories. Part II: Thermodynamic Phase Characteristics, J. Appl. Meteor. Climatol., 50, 645-661, https://doi.org/10.1175/2010jamc2468.1, 2011.
Shupe, M. D., Matrosov, S. Y., and Uttal, T.: Arctic mixed-phase cloud properties derived from surface-based sensors at SHEBA, J. Atmos. Sci., 63, 697-711, https://doi.org/10.1175/Jas3659.1, 2006.
Shupe, M. D., Daniel, J. S., de Boer, G., Eloranta, E. W., Kollias, P., Long, C. N., Luke, E. P., Turner, D. D., and Verlinde, J.: A FOCUS ON MIXED-PHASE CLOUDS The Status of Ground-Based Observational Methods, Bull. Am. Meteorol. Soc., 89, 1549-+, https://doi.org/10.1175/2008bams2378.1, 2008.
Silber, I.: Arctic Cloud-Base Ice Precipitation Properties Retrieved Using Bayesian Inference, J. Geophys. Res.-Atmos., 128, e2022JD038202, https://doi.org/10.1029/2022JD038202, 2023.
Silber, I., Fridlind, A. M., Ackerman, A. S., Knopf, D. A., Riemer, N., and Arabas, S.: AC-1D (1.0) [Software] https://doi.org/10.5281/zenodo.7108690, 2022.
Silber, I., Fridlind, A. M., Verlinde, J., Ackerman, A. S., Cesana, G., and Knopf, D. A.: The prevalence of precipitation from polar supercooled clouds, Atmos. Chem. Phys., 21, 3949-3971, https://doi.org/10.5194/acp-21-3949-2021, 2021.
Solomon, A., Feingold, G., and Shupe, M. D.: The role of ice nuclei recycling in the maintenance of cloud ice in Arctic mixed-phase stratocumulus, Atmos. Chem. Phys., 15, 10631-10643, https://doi.org/10.5194/acp-15-10631-2015, 2015.
Srivastava, D., Vu, T. V., Tong, S. R., Shi, Z. B., and Harrison, R. M.: Formation of secondary organic aerosols from anthropogenic precursors in laboratory studies, npj clim. atmos. sci., 5, 22, https://doi.org/10.1038/s41612-022-00238-6, 2022.
Stevens, D. E., Ackerman, A. S., and Bretherton, C. S.: Effects of Domain Size and Numerical Resolution on the Simulation of Shallow Cumulus Convection, J. Atmos. Sci., 59, 3285-3301, https://doi.org/10.1175/1520-0469(2002)059<3285:Eodsan>2.0.Co;2, 2002.

https://doi.org/10.5194/egusphere-2025-3620
Preprint. Discussion started: 6 October 2025

Stroeve, J. C., Kattsov, V., Barrett, A., Serreze, M., Pavlova, T., Holland, M., and Meier, W. N.: Trends in Arctic sea ice extent from CMIP5, CMIP3 and observations, Geophys. Res. Lett., 39, https://doi.org/10.1029/2012gl052676, 2012.

Sun, Y., Fridlind, A., Silber, I., Riemer, N., and Knopf, D. A.: Model code and sensitivity tests supporting "Prognostic simulations of mixed-phase clouds with model 1D-AC v1.0: The impact of freezing parameterizations on ice crystal budgets" (1.0) [Software] Zenodo, http://doi.org/10.5281/zenodo.16414825, 2025a.

Sun, Y., Fridlind, A., Silber, I., Riemer, N., and Knopf, D. A.: Output data from simulations supporting "Prognostic simulations of mixed-phase clouds with model 1D-AC v1.0: The impact of freezing parameterizations on ice crystal budgets" (1.0) [Dataset] Zenodo, http://doi.org/10.5281/zenodo.16413525, 2025b.

Sun, Y., Fridlind, A., Silber, I., Riemer, N., and Knopf, D. A.: Analysis scripts and figure generation code supporting "Prognostic simulations of mixed-phase clouds with model 1D-AC v1.0: The impact of freezing parameterizations on ice crystal budgets" (1.0) [Software] Zenodo, http://doi.org/10.5281/zenodo.16414282, 2025c.

Tully, C., Neubauer, D., and Lohmann, U.: Assessing predicted cirrus ice properties between two deterministic ice formation parameterizations, Geosci. Model Dev., 16, 2957-2973, https://doi.org/10.5194/gmd-16-2957-2023, 2023.

Udisti, R., Traversi, R., Becagli, S., Tomasi, C., Mazzola, M., Lupi, A., and Quinn, P. K.: Arctic Aerosols, in: Physics and Chemistry of the Arctic Atmosphere, edited by: Kokhanovsky, A., and Tomasi, C., Springer Polar Sciences, 209-329, https://doi.org/10.1007/978-3-030-33566-3_4, 2020.

Ullrich, R., Hoose, C., Möhler, O., Niemand, M., Wagner, R., Höhler, K., Hiranuma, N., Saathoff, H., and Leisner, T.: A New Ice Nucleation Active Site Parameterization for Desert Dust and Soot, J. Atmos. Sci., 74, 699-717, https://doi.org/10.1175/Jas-D-16-0074.1, 2017.

Vali, G.: Quantitative Evaluation of Experimental Results an the Heterogeneous Freezing Nucleation of Supercooled Liquids, Journal of the Atmospheric Sciences, 28, 402-409, https://doi.org/10.1175/1520-0469(1971)028<0402:Qeoera>2.0.Co;2, 1971.

Vali, G.: Interpretation of freezing nucleation experiments: singular and stochastic; sites and surfaces, Atmos. Chem. Phys., 14, 5271-5294, https://doi.org/10.5194/acp-14-5271-2014, 2014.

Vali, G., DeMott, P. J., Mohler, O., and Whale, T. F.: Technical Note: A proposal for ice nucleation terminology, Atmos. Chem. Phys., 15, 10263-10270, https://doi.org/10.5194/acp-15-10263-2015, 2015.

Vergara-Temprado, J., Murray, B. J., Wilson, T. W., O'Sullivan, D., Browse, J., Pringle, K. J., Ardon-Dryer, K., Bertram, A. K., Burrows, S. M., Ceburnis, D., DeMott, P. J., Mason, R. H., O'Dowd, C. D., Rinaldi, M., and Carslaw, K. S.: Contribution of feldspar and marine organic aerosols to global ice nucleating particle concentrations, Atmos. Chem. Phys., 17, 3637-3658, https://doi.org/10.5194/acp-17-3637-2017, 2017.

Verlinde, J., Harrington, J. Y., McFarquhar, G. M., Yannuzzi, V. T., Avramov, A., Greenberg, S., Johnson, N., Zhang, G., Poellot, M. R., Mather, J. H., Turner, D. D., Eloranta, E. W., Zak, B. D., Prenni, A. J., Daniel, J. S., Kok, G. L., Tobin, D. C., Holz, R., Sassen, K., Spangenberg, D., Minnis, P., Tooman, T. P., Ivey, M. D., Richardson, S. J., Bahrmann, C. P., Shupe, M., DeMott, P. J., Heymsfield, A. J., and Schofield, R.: The mixed-phase Arctic cloud experiment, Bull. Am. Meteorol. Soc., 88, 205-221, https://doi.org/10.1175/Bams-88-2-205, 2007.

Waman, D., Deshmukh, A., Jadav, A., Patade, S., Gautam, M., Phillips, V., Bansemer, A., and Jakobssonc, J.: Effects from Time Dependence of Ice Nucleus Activity for Contrasting Cloud Types, J. Atmos. Sci., 80, 2013-2039, https://doi.org/10.1175/Jas-D-22-0187.1, 2023.

Wang, B. B., Lambe, A. T., Massoli, P., Onasch, T. B., Davidovits, P., Worsnop, D. R., and Knopf, D. A.: The deposition ice nucleation and immersion freezing potential of amorphous secondary organic aerosol: Pathways for ice and mixed-phase cloud formation, J. Geophys. Res.-Atmos., 117, https://doi.org/10.1029/2012jd018063, 2012a.

Wang, B. B., Laskin, A., Roedel, T., Gilles, M. K., Moffet, R. C., Tivanski, A. V., and Knopf, D. A.: Heterogeneous ice nucleation and water uptake by field-collected atmospheric particles below 273 K, J. Geophys. Res.-Atmos., 117, https://doi.org/10.1029/2012jd017446, 2012b.

Westbrook, C. D. and Illingworth, A. J.: The formation of ice in a long-lived supercooled layer cloud, Quart. J. Roy. Meteor. Soc., 139, 2209-2221, https://doi.org/10.1002/qj.2096, 2013.

Wilson, T. W., Ladino, L. A., Alpert, P. A., Breckels, M. N., Brooks, I. M., Browse, J., Burrows, S. M., Carslaw, K. S., Huffman, J. A., Judd, C., Kilthau, W. P., Mason, R. H., McFiggans, G., Miller, L. A., Najera, J. J., Polishchuk, E., Rae, S., Schiller, C. L., Si, M., Temprado, J. V., Whale, T. F., Wong, J. P., Wurl, O., Yakobi-Hancock, J. D., Abbatt, J. P., Aller, J. Y., Bertram, A. K., Knopf, D. A., and Murray, B. J.: A marine biogenic source of atmospheric ice-nucleating particles, Nature, 525, 234-238, https://doi.org/10.1038/nature14986, 2015.

Xue, J., Zhang, T., Park, K., Yan, J., Yoon, Y. J., Park, J., and Wang, B.: Diverse sources and aging change the mixing state and ice nucleation properties of aerosol particles over the western Pacific and Southern Ocean, Atmos. Chem. Phys., 24, 7731-7754, https://doi.org/10.5194/acp-24-7731-2024, 2024.

Yang, F., Ovchinnikov, M., and Shaw, R. A.: Minimalist model of ice microphysics in mixed-phase stratiform clouds, Geophys. Res. Lett., 40, 3756-3760, https://doi.org/10.1002/grl.50700, 2013.

Zhao, X., Liu, X. H., Burrows, S. M., and Shi, Y.: Effects of marine organic aerosols as sources of immersion-mode ice-nucleating particles on high-latitude mixed-phase clouds, Atmos. Chem. Phys., 21, 2305-2327, https://doi.org/10.5194/acp-21-2305-2021, 2021.

Zhao, X., Liu, X. H., Burrows, S., DeMott, P. J., Diao, M. H., McFarquhar, G. M., Patade, S., Phillips, V., Roberts, G. C., Sanchez, K. J., Shi, Y., and Zhang, M.: Important Ice Processes Are Missed by the Community Earth System Model in Southern Ocean Mixed-Phase

https://doi.org/10.5194/egusphere-2025-3620
Preprint. Discussion started: 6 October 2025

Clouds: Bridging SOCRATES Observations to Model Developments, J. Geophys. Res.-Atmos., 128, e2022JD037513, https://doi.org/10.1029/2022JD037513, 2023.
Zuidema, P., Baker, B., Han, Y., Intrieri, J., Key, J., Lawson, P., Matrosov, S., Shupe, M., Stone, R., and Uttal, T.: An arctic springtime mixed-phase cloudy boundary layer observed during SHEBA, J. Atmos. Sci., 62, 160-176, https://doi.org/10.1175/Jas-3368.1, 2005.